NASA CR-134733

ORDERED STRUCTURES AND JET NOISE

by R. A. Petersen, R. E. Kaplan, and J. Laufer

UNIVERSITY OF SOUTHERN CALIFORNIA

prepared for

NATIONAL AERONAUTICS AND SPACE ADMINISTRATION

NASA Lewis Research Center

Contract NAS3-17857

1. Report No.	2. Government Accession No.	3. Recipient's Catalog No.
NASA CR-134733		

4. Title and Subtitle	5. Report Date
ORDERED STRUCTURES AND JET NOISE (U)	October 1974
	6. Performing Organization Code

7. Author(s)	8. Performing Organization Report No.
R. A. Peterson, R. E. Kaplan, J. Laufer	
	10. Work Unit No.

9. Performing Organization Name and Address	11. Contract or Grant No.
University of Southern California Department of Aerospace Engineering University Park Los Angeles, California 90007 USA	NAS3-17857
	13. Type of Report and Period Covered
12. Sponsoring Agency Name and Address	Contractor Report
National Aeronautics and Space Administration Washington, D. C. 20546	14. Sponsoring Agency Code

15. Supplementary Notes

Project Manager, Robert G. Dorsch, V/STOL and Noise Division, NASA Lewis Research Center, Cleveland, Ohio

16. Abstract

A series of measurements of near field pressures and turbulent velocity fluctuations were made in a jet having a Reynolds number of about 50,000 in order to investigate more quantitatively the character and behaviour of the large scale structures and to ascertain their importance to the jet noise problem. Time-averaging techniques alone are insufficient to detect interaction between the structures. As a consequence, a completely new statistical technique has been initiated in order to study this problem.

It was found that the process of interaction between vortices can be inhibited by artificially exciting the shear layers with periodic disturbances of certain frequency. The turbulent fluctuation amplitudes measured at four diameters downstream decreased considerably.

Finally, it was observed that the passage frequency of the structures decreased with x in a similar manner as the frequency corresponding to the maximum intensity radiation emanating from the same value of x.

The work is incomplete in the sense that no convincing direct connection between far field sound and the large scale structures in the flow has been demonstrated. (U)

17. Key Words (Suggested by Author(s))	18. Distribution Statement
Jet noise Shear layer turbulence Stochastic measuring techniques	Unclassified - unlimited

19. Security Classif. (of this report)	20. Security Classif. (of this page)	21. No. of Pages	22. Price*
Unclassified	Unclassified	55	$3.00

*For sale by the National Technical Information Service, Springfield, Virginia 22151

FOREWORD

The investigation conducted at USC concerning the role of the large scale, quasi-ordered structures of a turbulent jet in the generation of noise has been jointly supported during the period of this contract by the Department of Transportation under grant number DOT-OS-00002 and the National Aeronautics and Space Administration. The research conducted under NASA Contract NAS3-17857 and reported herein emphasizes those aspects of the problem that are related to the near rather than far field. The structure and content of this report reflects this fact.

TABLE OF CONTENTS

SUMMARY

Previous flow visualizations of turbulent jets at low Reynolds numbers have clearly indicated the presence of vortex ring-like structures and the nature of their interaction.

A series of measurements of near field pressures and turbulent velocity fluctuations were made in a jet having a Reynolds number of about 50,000 in order to investigate more quantitatively the character and behaviour of these structures and to ascertain their importance to the jet noise problem.

Auto- and cross-correlation measurements of the pressure fluctuations just outside of the jet yielded information about the average separation distance between neighboring structures and their convection velocity.

Coalescence between neighboring structures near the nozzle was detected by auto-correlation and two-point eduction techniques, however, its detection further downstream proved to be unsuccessful. As a consequence, a completely new statistical technique has been initiated in order to study this problem.

It was found that the process of interaction between vortices can be inhibited by artificially exciting the shear layers with periodic disturbances of certain frequency. The turbulent fluctuation amplitudes measured at four diameters downstream decreased considerably.

Finally, it was observed that the passage frequency of the structures decreased with x in a similar manner as the frequency corresponding to the maximum intensity radiation emanating from the same value of x.

The work is incomplete in the sense that whereas some new information was found about the large scale structures of jet turbulence, little quantitative information about their spatial character and their mutual interaction could be obtained; furthermore, as yet no convincing direct connection between far field sound and the large scale structures in the flow could be demonstrated.

INTRODUCTION

For the past two decades, jet noise research has been dominated by the work of Lighthill (ref. 1). In his theory the jet is modeled as a passive fluid medium with sound speed a_0, containing a distribution of "equivalent" acoustic sources whose strength is equal to the scalar contraction of the local fluid stresses present in the jet. The density field, ρ, must then satisfy the acoustic wave equation (ref. 1):

$$\frac{\partial^2 \rho}{\partial t^2} - a_0^2 \frac{\partial^2 \rho}{\partial x_k \partial x_k} = \frac{\partial^2 T_{ij}}{\partial x_i \partial x_j}$$

In Lighthill's model the fluid stress, T_{ij}, is considered to be distributed over a large number of random, uncorrelated "eddies".

There is a growing body of evidence indicating the existence of large organized structures within turbulent shear flows. Most recently in a Ph.D. thesis at the Rhein-Westfalia University, Aachen, West Germany, Gunther Neuwerth has demonstrated the presence of large coherent structures in a jet at high subsonic Mach numbers using an ingenious multispark Schlieren system (private communication). Although it is still an open question whether or not these structures contribute directly to the far field noise, one can make reasonable arguments that they might.

In an important recent work Crow and Champagne (ref. 2) detected large scale organized structures in a jet up to a Reynolds number of about 80,000 by visualization techniques. Furthermore, they used acoustically driven stagnation chamber resonances to excite the jet (Re = 100,000). They measured the jet response by placing a hot wire anemometer within the irrotational core where velocity perturbations would, presumably, reflect gross features of the local shear layer turbulence. They observed that the natural peak frequency occurred at a Strouhal number (based on jet exit velocity and exit diameter) of 0.3 and near the end of the potential core (x/D = 4). However, when the jet was excited at the first harmonic (St = .6), the fundamental was amplified at a still greater rate.

On the basis of their results, Crow and Champagne tended to regard the jet flow in terms of a column instability. In fact, in an unpublished work Crow formulated a "wave antenna model" in place of Lighthill's compact, random source model, in order to estimate the far field noise of a turbulent jet.

However, the presence of the large scale structures might be interpreted in terms other than that of wave instabilities. The measurements of Lau, Fisher and Fuchs (ref. 3) indicate that the shear layer is made up of a "row" of discrete rings of vorticity. This is consistent with the visualization of Winant and Browand (ref. 4) made in a two-dimensional free mixing layer. They found that due to the linear wave instability present near the origin of the shear layer, the initial vortex shear layer rolls up into cylindrical lumps of concentrated vorticity and the adjacent lumps roll around each other and coalesce into a single large lump. This "pairing" process was postulated as the major mechanism of turbulent shear layer growth. Vortex pairing has also been observed by Rockwell and Niccolls (ref. 5) in a two-dimensional jet using low Reynolds number flow visualization techniques and by Browand in an axisymmetric water jet as reported by Laufer (ref. 6).

There are well justifiable reasons for investigating vortex ring coalescence as a possible mechanism of far field noise production. Powell has shown (ref. 7) that when a free vortex ring stretches, it radiates acoustically like a dipole and the far field particle velocities are proportional to the second time derivative of its Kelvin impulse. During a pairing between two rings, the absence of an external force demands the Kelvin impulse of the pair is invariant. However, their far field, because of the Stokes effect, degenerates into a quadrupole-like behaviour.

On the basis of the preceeding discussion it is apparent that the question of the large scale structures as potential "acoustic" sources is a relevant one indeed. The principal aim of the research described in the present report is directed toward a detailed study of this question. For this purpose it is necessary to develop techniques for the detection of the organized structures inside the jet while simultaneously measuring their contributions to the far field noise. One should remark at this point that conventional cross correlation techniques involving one transducer in the flow and one in the far field are not particularly helpful, since single point flow measurements cannot provide sufficient information about the large structures.

The experimental problem has been approached in three parts. First, the behaviour of the large structures has been studied with particular emphasis on how their presence is related to the near field pressure and velocity signatures. In connection with this study the effect of artifically introduced disturbances near the initial jet development has also been included. Second, specific features of the radiated noise using a reflector microphone technique have been explored (primarily under DOT sponsorship). Finally, a search for a technique to relate the large scale structures to the noise field was undertaken.

In the first part of the Results and Discussion section, it is shown that the flow visualization techniques work well in detecting the behaviour of the large scale coherent structures in low Reynolds number jets. However, difficulties arise for moderate and high Reynolds numbers and the following two subsections describe the various approaches and techniques applied in an attempt to bring to light the characteristic features of the coherent structures by means of near field measurements. The subsequent discussion includes results obtained by the application of initial disturbances artificially introduced near the nozzle exit. Finally, measurements obtained primarily with a reflector microphone technique are presented with particular emphasis on how these measurements might relate to the large scale structures.

FACILITY AND INSTRUMENTATION

Model Jet

Most of the experiments described in this report have been carried out in a low speed jet facility. It consists of a vacuum cleaner blower, a settling chamber with damping screens and a contraction section with a circular nozzle. The contraction ratio is 36:1 and the nozzle diameter is 2.54 cm. The attainable maximum jet velocity is 70 m/sec, but most of the work was carried out at velocities near 30 m/sec. This corresponds to a Reynolds number based on exit velocity and nozzle diameter of 5.2×10^4.

The exit boundary layer is estimated to be less than .05 diameter. The exit mean velocity was found to be flat to better than 0.5% and the exit plane turbulence level was measured at 0.3%. This relatively high level was considered satisfactory for the experiments planned in the facility.

Anechoic Chamber

Far field measurements quoted in this report were carried out in the USC Anechoic Chamber facility under the sponsorship of the Department of Transportation (ref. 8). Briefly, the facility is of a blowdown type consisting of 1 or 2 inch jet nozzles with carefully designed valving and settling chambers exiting into a large anechoic chamber. Additionally, provisions have been included for extensive monitoring and measurement of the parameters which have been of importance for characterizing the properties of the turbulent jet.

Directional Microphone System

The directional microphone system is based on the imaging property of a spherical reflector. The reflector used has a radius of curvature of 53" and an aperature of 36". The dimensions were chosen after a parametric study of the imaging properties of spherical reflectors. A 1/8" B & K condenser microphone is used to pick up the focused acoustic waves at the geometrical image point.

The reflector disc is made of aluminum plate backed by another aluminum disc with rubber like material sandwiched in between to damp out the natural vibration of the primary disc. A gun-sight telescope is mounted at the back through the center of the reflector for alignment purpose.

Fig. 1 shows a schematic diagram of the traversing mechanism and the directional microphone system. This mechanism enables the directional microphone to scan automatically along the jet axis from a fixed location in the far field. At prescribed directions, the mechanism will pause for a few seconds to allow data to be recorded on tape before changing direction. The system also provides automatic refocusing at each prescribed direction. The scanning and refocusing are governed by a special electronic command system designed and built in our department.

Instrumentation

Mean velocity measurements were made with a pitot tube and traversing mechanism. Pitot tube total pressure was recorded off a capacitance-type differential pressure transducer.

Near field pressure measurements were made using 1/8" capacitor microphones with a nominal sensitivity of -80 dB re. 1 V/μbar. Microphone output was preamplified by a cathode follower.

Shear layer measurements were made with constant temperature hot wire anemometers. Typically the overheat ratio was 2, the wire was .0001 inch diameter Platinum, and the aspect-ratio was 400. In the presence of a large ratio

of mean velocity to r.m.s. fluctuation velocity, the wire responds to the velocity component parallel to the mean flow. Consequently, a single wire was sufficient to record axial velocity fluctuations. A cross wire arrangement was used when it was necessary to decompose the turbulence into axial and radial components. In all cases King's law, $E^2 = A + B\ (u \cos \theta)^{\frac{1}{2}}$ was assumed for calibration purposes, where $E(t)$ is the hot wire signal; $u(t)$ is the flow speed; $\theta(t)$ is the angle between the velocity and the normal to hot wire and A, B are constants of calibration. In the case of the crossed wire probe it is necessary to add and subtract the outputs of the two wires in a prescribed manner to derive the orthogonal velocity components.

Most of the statistical data processing was performed digitally using both hard wired equipment and a general purpose computer. Correlations and simple signal eductions were accomplished on a digital correlator, an instrument which had the capability of performing both auto-and cross-correlations, as well as signal recovery used for conditionally sampled time averages. An oscilloscope was adjusted to trigger on the slope and level of a reference signal, and the "gate out" was used to drive the "external trigger" on the correlator; for each trigger the correlator would average one frame of the data. In this way superimposed randomness would average to zero in favor of any wave form with a constant phase relative to the trigger condition. More sophisticated statistical analysis, such as joint probability distributions, was accomplished using the general purpose digital computer. Raw signal and calibration data were converted from continuous analog records to periodically sampled digitized records using an analog to digital converter subsystem of our own design.

MEASUREMENTS AND TECHNIQUES

Velocity

Mean velocities were measured with the Pitot tube apparatus using standard techniques while fluctuation measurements were carried out with the constant temperature hot wires discussed in the previous section.

Near Field Pressure

There is always some question as to what a microphone measures in the presence of mean flow. Work by Siddon (ref. 9) and Fuchs (ref. 10) have indicated that there are flow configurations where microphones can record the static pressure fluctuations with sufficient accuracy. The microphones were placed just outside the edge of the jet where mean velocities were small, and were oriented so that the plane of the diaphragm was roughly parallel to the mean flow.

Auto-correlations and cross-correlations of pressure signals were measured using the digital correlator. The microphones were located on the surface of a 10° cone intersecting the inside diameter of the

nozzle exit. Auto-correlations are shown at various downstream stations in Fig. 2. The r.m.s. level at each station is normalized to unity. Cross-correlations were measured with two microphones displaced a known distance. A displacement of 0.5 cm was selected for axial cross-correlations (Fig. 3)$_b$ while azimuthal cross-correlations were measured along a cone angle of 10^b (Fig. 4).

Special Statistical Techniques

Experience indicates that the unambiguous detection of large, coherent structures inside the shear layer is a difficult problem in signal recovery, especially downstream of the potential core. Time averaged techniques have proven successful only in detecting the first pairing; beyond that we have applied various eduction schemes developed recently at USC in connection with boundary layer and free shear layer research.

Two Point Eduction.- In order to measure phase relationships internal to a coherent structure at various depths in the shear layer, two point eduction was used. This technique, identical to that used by Winant and Browand (ref. 4), consists of sampling the properties of a large number of events occurring at a fixed position and at known time intervals before or after the occurrence of some judiciously chosen trigger conditions, measured at a different station and characteristic of the organized structure. Trigger position was inside the potential core, but close to the shear layer. The trigger condition selected was a positive signal slope and a signal level corresponding to one r.m.s. of the local fluctuation above the mean. This condition is a standard first attempt in conditional sampling of turbulent shear flows (ref. 23). At each station educted waveforms were recovered at the same downstream position but at varying radial positions. Educted waveforms appear in Fig. 5. Each figure corresponds to a particular downstream station, and in each case the indicated radial positions are relative, with positive positions in the direction of the entrainment region.

Joint Probability Measurements.- Although it is not possible to discern large scale turbulent patterns from single point measurements, it is possible to detect deterministic "subprocesses" in the turbulence from the joint statistics of orthogonal velocity components. The measurements were taken at the station $x/D = 2$, where the shear layer was fully turbulent, but where the vortex ring core was still reasonably localized so that there was room for vortex spreading. Two radial positions were chosen: $r/D = .49$ and $.56$ corresponding to $\bar{u}(r)/U_e = .79$ and $.60$, respectively.

The crossed wire probe was used to decompose the turbulence into radial and axial components. The hot wire signals were recorded on magnetic tape and then converted to a digital record for processing. From recorded calibration data, the digital records were linearized and stored as parallel records of radial (u_r) and axial (u_x) velocities. Velocity space was divided into

2500 cells and the fraction of the total time the record occupied a given cell (u_x, u_r) is the joint probability distribution $P(u_x, u_r)$ evaluated at the cell and normalized by the peak value of the distribution. The resulting joint probability distributions are shown in Fig. 6. The closed curves are contours of equal probability. The origin of the coordinate axes is the mean velocity $(\bar{u}_x, \bar{u}_r)$. Generally speaking, the distributions consist of a single peak with a ridge, indicated as a dashed line, connecting the first and third quadrants.

Time averages of the turbulence can be computed as moments of the joint probability distribution. Specifically mean velocities are defined

$$\bar{u}_i = \iint_{-\infty}^{\infty} u_i \, P(\underline{u}) \, d^2\underline{u} \tag{1}$$

variances are defined

$$\sigma_i^2 = \iint_{-\infty}^{\infty} [u_i^2 - \bar{u}_i^2] \, P(\underline{u}) \, d^2\underline{u} \tag{2}$$

and stresses are defined

$$\overline{u_i u_j} = \iint_{-\infty}^{\infty} [u_i u_j - \bar{u}_i \bar{u}_j] \, P(\underline{u}) \, d^2\underline{u} \tag{3}$$

Note that the probability distribution is normalized so that

$$\iint_{-\infty}^{\infty} P(\underline{u}) \, d\underline{u}^2 = 1 \tag{4}$$

and hence, the correlation coefficient is defined

$$R \equiv \overline{u_x u_r} / u_x' u_r' \tag{5}$$

Disturbance Generator

The experiments of Crow and Champagne (ref. 2) show that gross properties of the jet, such as axial velocity distribution, can be influenced by controlling the initial conditions of the jet. Their forcing technique, (acoustically driven stagnation chamber resonance) changes the shear layer structure directly since periodic exit plane modulation fluctuations induce a periodic series of ring vortices, a technique typically requiring forcing levels in excess of $0.01 U_e$.

An early attempt was made to thermally drive the model air jet shear layer with an axisymmetric glow discharge. This approach was subsequently abandoned due to the great difficulty in creating a uniform flow at atmospheric pressures.

More success was attained in driving the jet acoustically. A hemispherical chamber was fitted outside the nozzle contour to induce disturbances in the shear layer by acoustic pressure perturbations. Two speakers were used to excite a pressure field in the chamber, which communicated to the shear layer via a narrow gap, as shown in Fig. 7. In this way, an attempt was made to control the shear layer structures indirectly by providing an annular shaped acoustic wavefront that surrounds the entrainment region of the jet and where wave number $\underline{k}$ is parallel to the jet axis. It was hoped that by driving the jet in this way, at the right frequency, a given vortex ring pairing could be phase locked with the acoustics, facilitating detection. This method of forcing is expected to differ qualitatively from driving the jet core directly.

RESULTS AND DISCUSSION

Nature of the Turbulent Jet

The model jet exhibits general properties that are in good agreement with previous results. The centerline mean velocity decay is shown in Fig. 8 and is compared to the recent data of Crow and Champagne (ref. 2). Furthermore the linear spreading rate of the jet in the initial stage of development is depicted in Fig. 9, while Fig. 10 gives two typical mean velocity profiles in this region.

The non-steady aspect of the flow field is, of course, the primary interest here. The conventional root-mean-square velocity fluctuations will be described in a subsequent section; the presence of randomly occurring vortical structures will be discussed first. The most dramatic evidence of the existence of these vortical structures comes from flow visualizations.

Two new, unpublished sequences of flow visualizations have been made in the laboratories at USC by Dr. F. K. Browand. The first of these is a film, in which the initial vorticity of the jet is marked with dye (in a manner similar to that used in ref. 4) and its agglomeration into turbulent vortex rings is observable. The pairing process of Ref. 4 is easily observable in this film in the form of interactions of neighboring rings and can be seen as Fig. 2 of ref. 6. The second series of observations involved hydrogen bubble tracers and show substantially the same phenomena, although with the added advantage of being capable of providing more quantitative information.

These visualizations of the unsteady turbulent structure of the jet motivated further research at higher Reynolds numbers.

The Coherent Structures and Their Near Field

Reynolds Number Effect.- As discussed in the previous section, visual techniques provide a convincing picture of the existence of the large scale, vortical structures and the process of their coalescence. At higher Reynolds numbers

(Re 15,000) visual techniques are much more difficult to use, and do not lend themselves easily for quantitative study. One might rely on the principle of Reynolds similarity in arguing that the general structure of the jet is not altered (the jet spreading angle is independent of the Reynolds number); the argument does not assure one that the shape and behavior of the large structures is the same for higher Reynolds number values. For this reason it is essential that one should develop alternate techniques for studying the large scale motion. It would be desirable to carry out these studies under high speed flow conditions where noise generation is readily detectable, keeping in mind that one's primary interest is establishing a connection between the large structures and the radiated noise. Because of the well known difficulties with using hot wire techniques at high speed, a compromise was made and a Reynolds number of about 50,000 was chosen for most of the reported measurements. It was noted namely that over a large Reynolds number range and at least down to values of 90,000 the normalized power spectral density of the overall radiated noise exhibits a similar behavior (Fig. 11). Although there is an observable shift of acoustic power from lower to higher frequencies with increasing Reynolds number, the location of the peak power is remarkably insensitive to Reynolds numbers under widely different experimental conditions. With the conjecture that the peak frequency is related to the time scale appropriate to the behaviour of an organized turbulent structure, one would expect to find the same type of structures in high and low Reynolds number jets. Admittedly this argument cannot be considered a conclusive one; nevertheless, if measurements at Re = 50,000 show a picture of the large scale structure consistent with that obtained at Re = 5,000, this fact gives one more confidence to accept the Reynolds similarity argument for still higher values of the Reynolds number.

Nature of the Large Structures.- It is a well accepted fact, based on past experience, that the understanding of conventional statistical measurements in a turbulent flow field is extremely difficult and that it is most helpful, if not necessary, to have a physical model in mind in order to interpret those measurements. In planning the experiments, as well as interpreting the results, the existence of large scale structures in the approximate form of interacting vortex rings was postulated and a consistency or contradiction with this picture was continually sought.

In attempting to characterize these structures, one would first of all like to obtain information about their average convection velocity and their linear dimension. Of the two, the first quantity is by far more easily obtained without ambiguity.

Average Convection Velocity.- In order to minimize the effect of the fine scale "eddies" always present within the shear layer, measurements were made in the potential flow surrounding the turbulent layer, where the "footprint" of the large structures are expected to be most prevalent. The pressure cross-correlation measurements shown in Fig. 3 provide the required information. The probe separation distance divided by the passage time, τ, of the turbulent structures moving from one probe to the other is the convection velocity. Here, τ, is identified with the delay time corresponding to the peak correlation amplitude in the figure. The distribution of the convection velocity normalized

by the jet exit velocity along the jet is shown in Fig. 12. Along the potential core the ratio is in good agreement with previous measurements (refs. 3, 16 and 17). Downstream of the potential core the convection velocity remains approximately one-half of the centerline velocity and therefore, decays asymptotically as $1/x$.

Length Scales Associated with the Structures.- Much more difficulty was encountered in attempting to obtain information concerning the average separation distance between neighboring structures and about their size. This is primarily due to the fact that according to the visual observations these structures coalesce randomly in space as they move downstream; this prevents one from establishing a reliable phase reference that is necessary to separate spatial and temporal variation of the structures exhibited by the velocity or pressure signatures. Nevertheless, some progress has been made in this direction.

Referring to the energy spectra of the velocity fluctuations obtained at the two outer edges of a shear layer (ref. 4), the energy peaks are found to correspond to the passage frequency of two already-combined vortices while the spectrum near the layer center exhibits a second peak at twice this frequency attributed to the passage frequency of the individual vortices. With this information in mind one would expect that in the near potential field of the jet where velocity and pressure fluctuations are closely correlated (refs. 3 and 17) the pressure spectra or the equivalent auto-correlations would give information about the time of passage between successive structures. The time delay to the first minimum of the auto-correlations of Fig. 2 is established as a measure of the average passage time between successive structures at various stations downstream of the nozzle (Fig. 13). With this information and from the knowledge of the convection velocity, an average separation distance, λ, between the structures can be calculated (Fig. 14). Separation λ increases linearly with downstream distance.

One should note here parenthetically, that it would be erroneous to identify the length λ with the size of the "acoustic" sources. Referring to the visual observations and to Powell's vortex source model (ref. 7), it is more reasonable to think of regions of high correlation (and high vorticity) as the coherent volume acting as the "acoustic" source. The dimension of this region is unlikely to be larger than the local shear layer thickness, and therefore, less than λ. Unfortunately, no successful technique was found with pressure or velocity transducers for a quantitative measurement of this length scale; perhaps, the use of a vorticity meter might prove to be more profitable.

Similarly, no additional information was provided by the pressure cross-correlations measured radially across the jet at positions lying on a cone angle of 10° (Fig. 4). The correlation is decreasing rapidly with axial distance from the nozzle and is essentially zero at about $x/D = 5$, in qualitative agreement with the results of Mollo-Christensen (ref. 18). In retrospect this is not surprising, since two pairing vortex rings are unlikely to retain axisymmetry; higher order modes are expected to develop in the turbulent region.

Coalescence and Shear Layer Growth.- Interaction between neighboring vortices referred to as coalescence has been postulated to be the major mechanism of shear layer growth (ref. 4). Subsequently, Laufer, Kaplan and Chu (ref. 19) conjectured that this interaction may be an essential contributor to the noise producing process. It is, therefore, of considerable importance to study this phenomenon.

The occurrence of the first pairing is demonstrated in the set of auto-correlations shown in Fig. 15, measured by placing a hot wire into the shear layer at the radial positions where the velocity fluctuations are maximum, a position which should select the peak of the eigenmode. At axial stations $0 < x/D < .5$ the auto-correlation looks like a damped oscillation with a Strouhal number of 0.23 based on the initial shear layer thickness of 0.05 diameters and on half of the jet velocity. This frequency corresponds to the eigenfrequency of the preferentially amplified, two dimensional shear layer instability. The implication is that the jet shear layer is essentially two dimensional near the exit plane, and the subsequent two dimensional instability grows with the shear layer until curvature effects force the local instabilities to phase lock into a growing axisymmetric vortex sheet. Further downstream, at $x/D > .7$ (Fig. 15), every other wave has disappeared. This is the completion of the first pairing and occurs after the transition of the shear layer to turbulent flow. It should be emphasized that this production of an exact subharmonic is qualitatively different from what would be observed if dissipation or diffusion were the important physical mechanism here. Both of these processes lack the necessary phase reference to produce the discontinuous spectral shift observed in Fig. 15. The continuous length scale spreading produced by turbulent diffusion would result in a continuous spectral shift, which is, in fact, observed beyond one diameter downstream. Consequently, beyond the first pairing, auto-correlation measurements are insufficient to distinguish between diffusion and pairing as the important mechanism in shear layer spreading.

In order to determine the phase relationship across the mean coherent structure at positions further downstream, two-point education, described in the section on Special Statistical Techniques was used. The educted waveforms are shown in Fig. 5. Close to the nozzle (Fig. 5a) there is an abrupt 180° phase shift in the center of the shear layer where the fluctuation amplitudes are small. This behaviour is suggestive of a simple vortex sheet. Another 0.1 diameter downstream, however, this behaviour has changed; the phase shift is spread out over 0.05 cm, and in the center there are twice as many crests (Fig. 5b). This result is consistent with the findings in the shear layer (ref. 4) where the double frequency is related to the pairing process. The double structure is barely discernable at $x/D = 0.9$ (Fig. 5c); thereafter, the phase shift appears smooth and continuous (Figs. 5d and 5e).

The failure of both of the above techniques to detect the coalescence at downstream positions larger than a diameter is believed to be primarily due to the phase jitter in pairing location. In order to get an estimate of the magnitude or standard deviation of the fluctuations in pairing location the following calculation has been carried out based on a simple model.

If we consider the coherent shear layer structures to be vortex rings, then the rate of vortex pairings within a given interval (x_1, x_2) is the rate $\dot{n}$ at which waves disappear in that interval,

$$\dot{n} = f(x_1) - f(x_2) \tag{6}$$

Here f is the vortex passage frequency (based on auto-correlation period, Fig. 13). From that figure, frequency decays as

$$f/f_o = D/x \tag{7}$$

along the first four diameters and

$$\dot{n} = f_o\left[\frac{D}{x_1} - \frac{D}{x_2}\right] \tag{8}$$

If $x_2 - x_1$ is the mean distance, $l(x)$, for one pairing to take place, then half the waves passing station x_1 will have disappeared before reaching station x_2 :

$$\tfrac{1}{2} f(x_1) = \dot{n}$$

so that

$$f_o/2(x/D) = \frac{f_o}{x/D} - \frac{f_o}{(x+l)/D} \tag{9}$$

and $l(x) = x$. Therefore if x_o is the mean location of the first pairing then the location of the n^{th} pairing will be

$$x_n/D = 2^{n-1}(x_o/D) \tag{10}$$

A similar analysis predicts mean pairing locations beyond the potential core. If the first pairing were located at $x_o = 0.24$ diameters, then the deduced pairing locations would be as follows:

n	1	2	3	4	5	6	7
x_n/D	.24	.68	1.9	4.4	6.3	8.9	12.6

Downstream of the jet core the pairings become increasingly sparse and, of the seven deduced pairing locations, only three (numbers 4 through 6) occur in the principal noise-producing regions of the jet (ref. 8). Then, according to this model, the majority of the noise would be produced by the fourth, fifth and sixth pairings.

Vortex pairing has been postulated to be the major mechanism of shear layer growth (ref. 4). The fact that jet shear layers are observed to grow linearly with x should permit an estimate of the upper limit to the phase jitter associated with pairing. If the location of the n^{th} pairing is assumed to follow a Gaussian distribution about its mean position, x_n, the shear layer thickness, $h(x)$, can be modeled as

$$h(x) = h_0 \left\{ 1 + \sum_{n=1}^{N} 2 A_n \int_0^x \exp\left[-(\xi - x_n)^2 / 2(\sigma \lambda_n)^2 \right] d\xi \right\} \qquad (11)$$

where

$$A_n = \left\{ \int_0^\infty \exp\left[-(\xi - x_n)^2 / 2(\sigma \lambda_n)^2 \right] \right\}^{-1}$$

and λ_n = Mean vortex spacing at position x_n ,

σ = Uncertainty in the pairing location expressed as a fraction of the local vortex spacing.

Equation (11) has been computed for the jet core region for three values of σ (Fig. 16a, b and c). The shear layer spread does not become smooth until σ is greater than 0.8; however, for $\sigma > 1.5$ the growth rate is slower than linear. On the basis of this model one would estimate the dispersion in pairing location to be of the order of the vortex spacing. This relatively large jitter can indeed explain the reason for the difficulties in studying the pairings by conventional statistical techniques.

Preliminary Results Using Markov Transitions

The most controversial feature of the two-point eductions is the selection of a relevant trigger condition. The simple condition of level and slope is sufficient for detecting mean structure, whereas detection of an intermittent event without a fixed phase relationship to the mean structure requires subtlety. A promising method, derived from pattern recognition techniques, is to study the appropriate joint probability distribution and transition operator in hopes of identifying some self-similar, deterministic subprocess associated with the turbulent structure of interest. Identification of the subprocess provides the necessary trigger condition for educing the structure with one or more signal probes separated in space from the trigger location. We postulate that for high Reynolds numbers the state of the fluid is completely described by the field $\underline{u}(\underline{x}, t)$, and that at a fixed position the future state of the fluid is described statistically by the present state; i.e. the turbulence may be represented as a model Markov process with a vector Langevin Equation

$$du_i = f_i \, dt + \sigma_{ij} \, d\beta_j \qquad (12)$$

The vector $\underline{f}$ is the time-averaged transition $\delta\underline{u} = \underline{u}(t + \delta t) - \underline{u}(t)$ given the state $(\underline{u}_x , u_r)$. It is referred to as the expected value of the transition and represented formally by

$$f_i \, \delta t = E\{ \delta u_i \mid \underline{u} \} \qquad (13)$$

The vector $\underline{\beta}$ is purely random with zero mean and unity variance. That is

$$E\{d\underline{\beta} | \underline{u}\} = 0 \tag{14a}$$

and

$$E\{d\beta_i \cdot d\beta_j | \underline{u}\} = \delta_{ij} \cdot dt \tag{14b}$$

The tensor $\underline{\underline{\sigma}}$ is a matrix of influence coefficients and when contracted against $d\underline{\beta}$ represents the Brownian motion of the fluid at a location $\underline{u}$, and δ_{ij} is the familiar Kroenecker delta. Taken together, $\sigma_{ij} d\beta_j$ represents the diffusion of the system state around a location $\underline{u}$ during a time step δt, and $\underline{f}\,\delta t$ represents the corresponding drift to the new average state.

It is useful here to present some statistics of the velocity components u_x and u_r as discussed in the part on Joint Probability Measurements. Their joint probability distribution taken at two points across the shear layer are given in Fig. 6. The distribution at $r/D = .56$ (Fig. 6a) is skewed towards positive velocity fluctuations u_x and u_r, indicating entrapment of high momentum, irrotational fluid from the core. In the third quadrant (negative u_x and u_r fluctuations) there is a well defined "edge" to the distribution which appears topographically like a "forbidden zone": There are a negligibly small number of occurrences of velocities with (u_x, u_r) values lower than this edge value, and the isoprobability contours are closely spaced near this edge. Hence the fluid velocity spends a good deal of time next to the edge but is rarely able to accelerate beyond it. The distribution measured closer to the potential core ($r/D = .49$, Fig. 6b) does not exhibit such an edge, but shows a general consistency in that it is skewed towards the negative u_x, u_r fluctuations. This distribution is dominated by entrainment of low momentum fluid from the outside of the jet.

The correlation coefficient R is tabulated in Table 1, along with r.m.s. values of u_x and u_r fluctuations. In Table 1, our results are compared against the low speed jet measurements of ref. 3, the jet measurements of Bradshaw, Ferriss and Johnson (ref. 20), and the two-dimensional shear layer measurements of Jones (ref. 21) and Liepmann and Laufer (ref. 22). There is a surprisingly broad spread among published values, but generally speaking our measured r.m.s. levels of fluctuating velocity components is in acceptable agreement while our correlation coefficients are slightly low.

The actual measurement of joint probability densities and state space transitions is a difficult process with analog equipment; however, these are among the easiest calculations to program for digital computers. In practice, records of u_x and u_r are sampled periodically and stored in parallel. Each occurrence of $\underline{u}$ in a box $(u_x \pm \Delta u_x/2\,;\ u_r \pm \Delta u_r/2)$ generates a unique index. By counting the number of such occurrences, the joint probability distribution is generated. At the same time one can look forward one step in time to produce the instantaneous differential $(\Delta u_x, \Delta u_r)$, which is

associated with the state-space location (u_x, u_r). The ensemble average of $\Delta \underline{u}$, determined at each state-space location $\underline{u}$, is just the transition operator $\underline{f}dt$. Higher order transition operators are measured in similar manner.

Two sets of measured transition vectors $\underline{f}$, obtained at the same two indicated points in the shear layer, are shown in Figs. 17 a and b. The transitions are indicated superimposed on isoprobability contours. In Fig. 17b generally they point radially towards the probability peak; i.e., the most probable transition will be towards the most probable state. However, in Fig. 17a, near the edge of the probability distribution, the transition vectors (when laid end-to-end) indicate a swirl-like pattern. It would be useful to develop a quantitative measure of such subprocesses. There are two that come readily to mind; the inner product $\underline{u} \cdot \underline{f}$ and the cross product $\underline{u} \times \underline{f}$. The latter would be particularly interesting since the integral

$$\iint_{-\infty}^{\infty} (\underline{u} \times \underline{f}) \, d^2\underline{u}$$

would provide a distributive measure of how much "swirl" is present. However, the quantity $\underline{u} \times \underline{f}$ has so far eluded our physical interpretation. The interpretation of $\underline{u} \cdot \underline{f}$ is much more straightforward, and is a direct consequence of the development of the study of joint transitions.

The Brownian motion of the system provides the leading term in the expectation value of the joint transition tensor $\delta u_i \, \delta u_j$

$$E\{\delta u_i \, \delta u_j \mid \underline{u}\} = \sigma_{ik} \sigma_{jk} \, \delta t + O(\delta t^2) \tag{15}$$

Note that Equations 13 and 15 are the Lindeborg conditions of a Markov process. It is a matter of simple algebra to show that the expected transition in the cross product $u_i u_j$ is

$$E\left\{ \frac{\delta (u_i u_j)}{\delta t} \middle| \underline{u} \right\} = \Sigma_{ij} + u_i f_j + u_j f_i \tag{16}$$

where the tensor $\underline{\Sigma}$ in the matrix product

$$\Sigma_{ij} \equiv \sigma_{ik} \sigma_{jk} \tag{17}$$

If Equation 16 is rewritten in terms of products of fluctuating components $\tilde{u}_i$, $\tilde{u}_j$ and contracted over the indices, then

$$E\left\{ \frac{\delta (\frac{1}{2} u_k u_k)}{\delta t} \middle| \underline{u} \right\} = \frac{1}{2} \Sigma_{kk} + u_k f_k \tag{18}$$

is the expected transition in turbulent kinetic energy. Note that $u_k f_k$ is the inner product discussed earlier. The contracted tensor

$$\delta t \, \Sigma_{kk} = E\{\delta u_k \, \delta u_k \mid \underline{u}\} \tag{19}$$

can be measured directly, and is insensitive to the coordinate system misalignment.

It is interesting to compare turbulent kinetic energy (T.K.E.) transitions with T.K.E. density probability distribution itself defined as $(u_x^2 + u_r^2) P(\underline{u})$. Fig. 18 shows isoprobability contours of T.K.E. density at $r/D = .56$, while Fig. 19 displays contours of equal values of T.K.E. transition (16) at the same radial position. Positive values of δ(T.K.E.) indicate transitions to levels of higher T.K.E. while the cross-hatched region denotes negative transitions. The distribution of T.K.E. transition levels is consistent with intuition in that regions of small T.K.E. (i.e. near the mean) show the largest positive δ(T.K.E.) and vice versa. In comparing Figs. 18 and 19, it is apparent that the T.K.E. peak associated with entrapment of high momentum fluid (positive u_x and u_r) occurs at a state corresponding to small rates of change of T.K.E. By implication, this fluid spends most of its time traveling between states of large positive and negative acceleration, which is what one would expect. However, the T.K.E. peak associated with low momentum fluctuations which exhibits a sharp "edge" like the $P(\underline{u})$ distribution, is located at a state where T.K.E. transition levels are large in magnitude. Apparently when a particle reaches the edge of the energy distribution, it experiences a large acceleration towards lower energy levels. This acceleration must be parallel to the edge and is consistent with the shape of the $P(\underline{u})$ ridge shown in Fig. 6a as a dotted line.

The set of data $P(\underline{u})$, $\underline{f}(\underline{u})$ and $\underline{\underline{\Sigma}}(\underline{u})$ provides a detailed and sensitive indicator to the state of the turbulent fluid. In contrast, both time correlations and spectra taken at the two locations cited show little difference or distinctive features. Both of these quantities can be extracted from $\underline{\underline{r}}$, $\underline{f}$, and $\underline{\Sigma}$, although with some difficulty.

The advantage to these measurements is that they provide inputs to newer theories of turbulent structure involving Markov processes, and hence can prove to be useful to the analyst.

Artificial Initial Disturbances

The experiments of Crow and Champagne (ref. 2) have shown that the gross properties of the jet, such as axial velocity distribution and spreading rate, can be influenced by controlling the initial conditions of the jet. Their forcing technique— acoustically driven stagnation chamber resonance – requires relatively high disturbance amplitudes, typically in excess of 1% of the jet exit velocity. The method adopted in the present work consisted of generating an annular shaped acoustic wavefront (Fig. 7) that surrounds the entrainment region of the jet and that has a wave number vector parallel to the jet axis. It was hoped that by driving the shear layer in this way, at the right frequency, a given vortex ring pairing could be phase locked with the disturbance, thus, facilitating detection.

Results have shown that the above described forcing technique apparently did inhibit the phase jitter but only during the first and possibly the second vortex pairing, by phase locking the laminar eigenmode. As a consequence, the transition to turbulence was delayed from 0.3 to 0.5 diameters.

Although this type of driving has no obvious influence over mean properties of the jet (such as axial and radial velocity profiles) there is an interesting influence over shear layer turbulence. Broadband turbulence levels in the transition region are increased by forcing, probably by strengthening the eigenmode. Further downstream, however, forcing is observed to decrease considerably the shear layer turbulence. Fig. 20 shows radial traverses of the forced and unforced shear layer at the downstream station $x/D = 4$. Forcing was at 3.6 kHz, (the laminar eigenmode) and the mean velocity profile is shown for orientation. The turbulence level is reduced by 50 % at the centerline and by 20 % at the peak value. It is to be noted that this result is in direct contrast to the effect observed by Crow and Champagne (Fig. 28, ref. 2). This observation emphasized that driving the jet core produces qualitative differences from driving the shear layer turbulence only.

It was, of course, of considerable interest to investigate whether or not the reduction in turbulence level effects the far pressure field. The above method of excitation was repeated, therefore, in a jet placed in the anechoic chamber. At a Mach number of 0.5 intensity and spectral measurements indicated no discernable change when the artificial disturbance was introduced into the shear layer. Instead of continuing the far field investigation, it was decided to attempt to understand in more detail the role played by the artificial disturbances in the near field.

Inter-Relationship Between the Large Structures and the Noise Field

As pointed out in the introduction, the question of the large scale structures as potential acoustic sources is a relevant one. A direct experimental confirmation of this problem is a most difficult one; the evolution in time of large coherent flow regions would have to be measured, (simultaneously with the far field pressure) a task that present techniques cannot as yet perform. A more indirect approach to the problem has been adopted in the present work: one postulates a feasible noise mechanism associated with the large structures and one makes certain measurements in the far field to look for the consequences of the assumed mechanism. This requires a highly directional microphone in order to be able to detect the noise generated over a relatively small region of the jet.

Assuming that one of the dominant mechanisms of the jet noise is associated with the coalescing vortical structures in the flow, one would expect to find certain features in the far field. In particular, one can think of at least three such characteristic features:

1. the noise produced by any single region of the jet ought to be intermittent;
2. evidence of spatial coherence should be present in the noise field, since the coalescence is a spatially coherent process;
3. the noise spectrum should reflect some characteristic time that is associated with the coalescence process.

In studying the data obtained with the directional microphone with respect to these features the following comments can be made. At subsonic jet velocities no intermittency has been observed in the far field; it is quite possible that at these velocities the intermittency is being obscured by the spatial averaging of the mirror's finite focusing window. It should be mentioned, however, that at supersonic velocities highly intermittent signals have been observed which in fact are believed to emanate from the large structures.

With respect to point 2, spatial coherence measurements have been made in the far field with a nine microphone array located at equally spaced intervals along the 36 in. line indicated in Fig. 21. Spatial coherence is expressed as cross-correlation coefficients with respect to the center microphone. Polar angles of 30^{o} and 90^{o} were chosen. Although moderate coherence has been found the evidence was judged to be inconclusive.

A more interesting result has been found related to the characteristic time of the coalescence. According to the model of Winant and Browand (ref. 4), the pairing time is proportional to the vortex size (which in turn is proportional to the vortex spacing) and inversely proportional to the convection speed. But the ratio of vortex separation distance to convection speed corresponds to the average passage time between successive vortices (Fig. 13). These data have been replotted in the form of a non-dimensional passage frequency in Fig. 22 and compared to the following far field measurements. Narrow band noise intensity distribution measurements were made with the reflector microphone located 90^{o} to the jet axis and directed toward narrow segments of the jet along its axis. Fig. 23 shows a set of intensity distributions as a function of x/D. It is seen that at a given x station one particular frequency (or Strouhal number) contains more energy than any other. These non-dimensional frequencies have been plotted as a function of x/D in Fig. 22. It is seen that the near and far field data show surprisingly similar trends. (Unfortunately, the accuracy of the far field measurements near the jet exit is limited by the spatial resolution problems.) This implies that the time scales associated with the noise radiated normally from a given region of the jet is related to a time scale associated with the near field temporal coherence. Clearly, such a conjecture is insufficient to provide a convincing argument to the above model and much more work is necessary to clarify this question.

CONCLUSIONS

Various statistical measurements carried out within and near a turbulent jet are shown to be consistent with the conjecture that large scale organized structures do exist in such a shear layer; they interact with each other consistent with visual observations made at low Reynolds numbers. Unfortunately, because of their random interaction by coalescence, only a limited amount of information about their nature and behaviour could be extracted even with the most modern statistical techniques.

In particular, the average separation distance between neighboring structures was obtained from conventional auto-and cross-correlation measurements. It was found to increase linearly with x along the jet axis.

The pairing process, clearly observable by visual techniques, could be detected only in its earliest stages; more sophisticated statistical methods, such as two-point eduction or state-space statistics were unable to identify the occurrence of coalescence further downstream in the flow. It is argued that the difficulty is primarily due to the random occurrence of the coalescence which prevents one from acquiring a reliable phase reference necessary for the detection.

The presence of the structures and the important consequences of their interaction was further brought out by artificial excitation of the jet. Although no measurable changes were detected in the mean velocity field of the jet, a considerable decrease in the velocity fluctuations could be attained at four diameters downstream of the jet. It is conjectured that a particular eigenmode of the shear layer can inhibit the interaction process between the vortex rings and thereby delay transition.

Finally, it should be noted that as yet the work has not yielded a technique that would allow one to study directly the connection, if any, between the large structure behaviour and the far field noise. The only circumstantial evidence produced by the present research is the observation that the passage frequency (which is believed to be proportional to the rate of subharmonic formation) of the structures varies with x in a surprisingly similar manner as the frequency corresponding to the maximum intensity radiation emanating from the same value of x. It is evident that this point, a most important one for understanding the jet noise problem, needs to be investigated in much more detail.

SYMBOLS

$\underline{a}$	sonic velocity
$\underline{a}_o$	sonic velocity - ambient
D	jet exit diameter
R	jet exit radius
f	wave frequency
$\underline{f}$	transition vector (expectation of velocity partial time derivative)
h(x)	jet shear layer thickness
$\underline{k}$	wave number
$M(\underline{x})$	local Mach number
M_o	local Mach number - referred to ambient
M_e	exit plane Mach number
$P(u_x, u_r)$	joint probability distribution
p(x)	static pressure fluctuation
p'	r.m.s. pressure fluctuation
R	correlation $\overline{u_x u_r} / u'_x u'_r$
Re	Reynolds number $U_e D/\nu$
T	near field time scale
$\underline{u}(\underline{x}, t)$	local velocity (tensor notation u_i)
u_x	local velocity - axial component
u_r	local velocity - radial component
$\tilde{u}_i(x, t)$	fluctuating local velocity = $u_i - \bar{u}_i$
u'_i	r.m.s. velocity fluctuation = $(\overline{u_i^2} - \bar{u}_i^2)^{\frac{1}{2}}$
u_g	average turbulence convection velocity
u_p	phase velocity
U(x)	jet centerline velocity
U_e	jet exit plane velocity
$\underline{x}$	field position vector

x	= axial position
r	= radial position
Δr	= difference in radial position from shear layer centerline
δQ	= $Q(t + \delta t) - Q(t)$ for any Q
$\underline{\underline{\Sigma}}$	state space joint transition tensor
θ	spherical polar angle
$\lambda(x)$	local wave length
ν	kinematic viscosity
$\rho(\underline{x})$	local density
σ	dimension uncertainty in vortex pairing location (Eq. 11)
$\underline{\sigma}$	expectation of square of velocity time derivative (tensor quantity σ_{ij})
τ	time delay
ϕ	azimuthal angle

REFERENCES

1. Lighthill, M.J., "On Sound Generated Aerodynamically: I General Theory", Proc. Roy. Soc., A211, (1952), 564-78.

2. Crow, S.C., and Champagne, F.H., "Orderly Structure in Jet Turbulence", J. Fl. Mech., 48 (1971), 547-91.

3. Lau, J.C., Fisher, M.J., and Fuchs, H.V., "The Intrinsic Structure of Turbulent Jets", J. Sound and Vib., 22 (1972), 379-406.

4. Winant, C.D., and Browand, F.K., "Vortex Pairing: The Mechanism of Turbulent Mixing-Layer Growth at Moderate Reynolds Number", J.F.M., 63 (1974), 237-56.

5. Rockwell, D.O., and Niccolls, W.O., "Natural Breakdown of Planar Jets", J. Basic Engr., Trans. ASME, D94 (Dec. 1972), 720-30.

6. Laufer, J., "New Trends in Experimental Turbulence Research", Ann. Rev. Fl. Mech., 7 (1975), (Annual Review, Inc.), To Be Published.

7. Powell, A., "Theory of Vortex Sound", JASA, 36 (1964), 177-95.

8. Laufer, J., Kaplan, R.E., and Chu, W.T., "Acoustic Modelling of the Jet Noise Abatement Study", Symposium on Transportation Noise Research, Stanford University, (1973).

9. Siddon, T.E., "On the Response of Pressure Measuring Instrumentation in Unsteady Flow", Univ. Toronto UTIAS Rep. 136, (1969).

10. Fuchs, H.V., "Measurements of Pressure Fluctuations Within Subsonic Turbulent Jets", J. Sound and Vib., 22 (1972), 361-78.

11. Howes, W.L., "Similarity of Far Noise Fields of Jets", NASA TR R-52, (1960).

12. Tyler, J.M., and Perry, E.C., "Jet Noise", SAE preprint no. 287, (1954).

13. Fitzpatrick, H.M., and Lee, R., "Measurements of Noise Radiated by Subsonic Air Jets", The David. W. Taylor Model Basin, Rept. 835, (1952).

14. Waterhouse, R.V., and Berendt, R.O., "Reverberation Chamber Study of the Sound Power Output of Subsonic Air Jets", JASA, 30 (1958), 114-21.

15. Rollin, V.G., "Effect of Jet Temperature on Jet Noise Generation", NACA TN 4217, (1958).

16. Ko, N.W.M., and Davies, P.O.A.L., "The Near Field Within the Potential Core of Subsonic Cold Jets", J.F.M., 50 (1971), 49-78.

REFERENCES (Cont.)

17. Fuchs, H., "Space Correlations of the Fluctuating Pressure in Subsonic Turbulent Jets", J. Sound and Vib., 23 (1972), 77-99.

18. Mollo-Christensen, E. "Jet Noise and Shear Flow Instability Seen from an Experimenter's Viewpoint", J. Appl. Mech, Trans. ASME, 34 (1967), 1-7.

19. Laufer, J., Kaplan, R.E., Chu, W.T., "On the Generation of Jet Noise", AGARD Specialists Meeting, "Noise Mechanisms", Preprint No. 131, Rhode-St.-Genese, Belgium, (1973).

20. Bradshaw, P., Ferriss, D.H., and Johnson, R.F. "Turbulence in the Noise-Producing Region of a Circular Jet", J.F.M., 19 (1964), 591-624.

21. Jones, I.S.F., "Fluctuating Turbulent Stresses in the Noise-Producing Region of a Jet", J.F.M., 36 (1969) 529-43.

22. Liepmann, H.W., and Laufer, J., "Investigation of Free Turbulent Mixing", NACA TN 1257, (1947).

23. Willmarth, W.W. and Lu, S.S., "Structure of Reynolds Stress Near the Wall", NATO-AGARD Conference Proc. 13, Technical Editing and Reproduction Ltd., London (1972).

TABLE 1

Comparison of Turbulence Levels

Jet Measurements	U_e m/sec	$\bar{u}/U_e = .60$ u_x'/U_e	u_r'/U_e	R	$\bar{u}/U_e = .79$ u_x'/U_e	u_x'/U_e	R
Present	27	.18	.11	.29	.15	.11	.43
Bradshaw, Ferriss, Johnson (Ref. 20)	M=.3	.14	.13	.53	.12	.12	
Lau, Fisher, Fuchs (Ref. 3)	61			.45			.5
2-Dimensional Shear Layer Measurements							
Jones (Ref. 21)	34.5	.18	.12		.16	.12	
Liepmann, Laufer (Ref. 22)	18.5	.26	.16	.54	.17	.12	.56

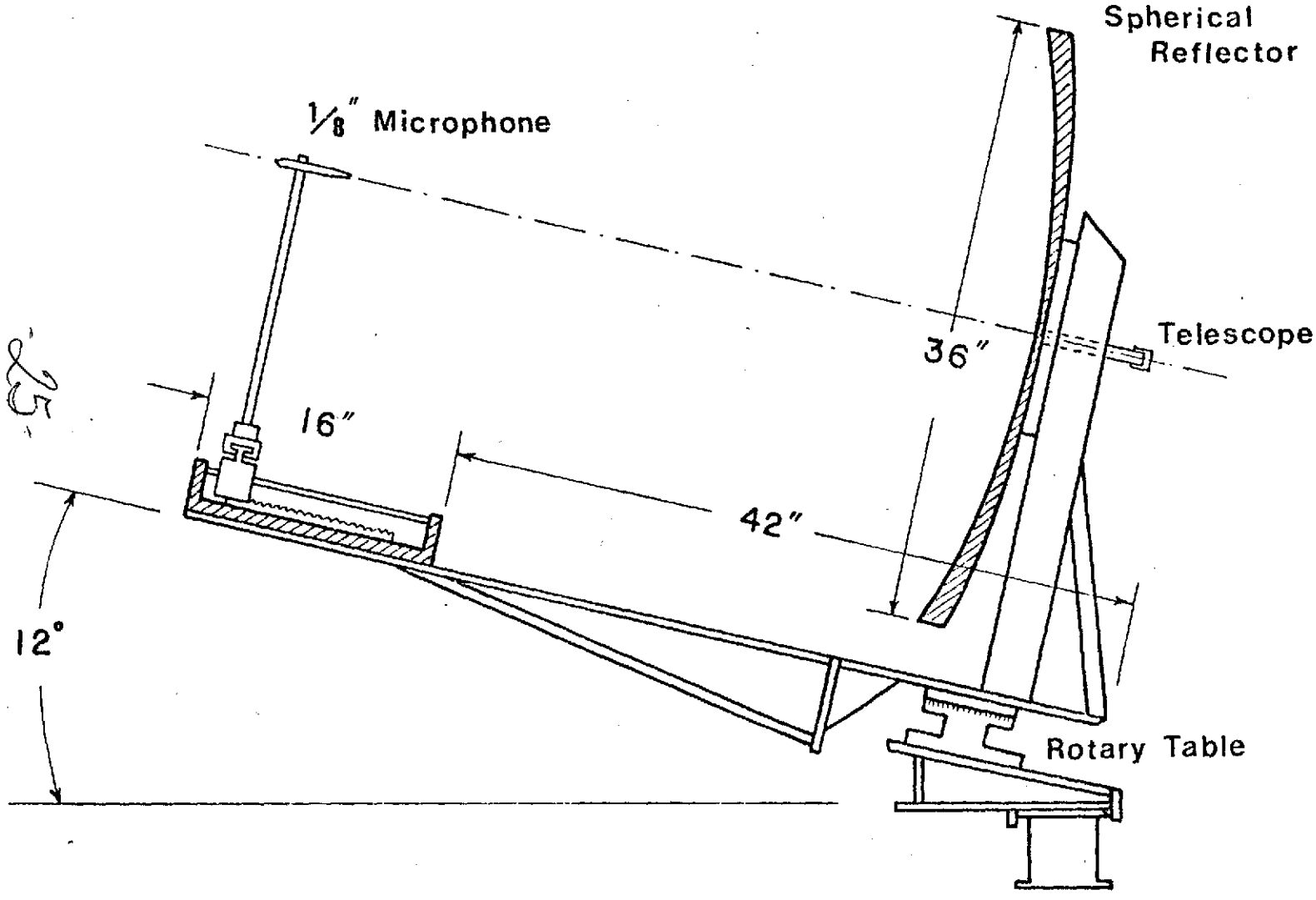

Fig. 1 Schematic Diagram of Reflector Microphone System

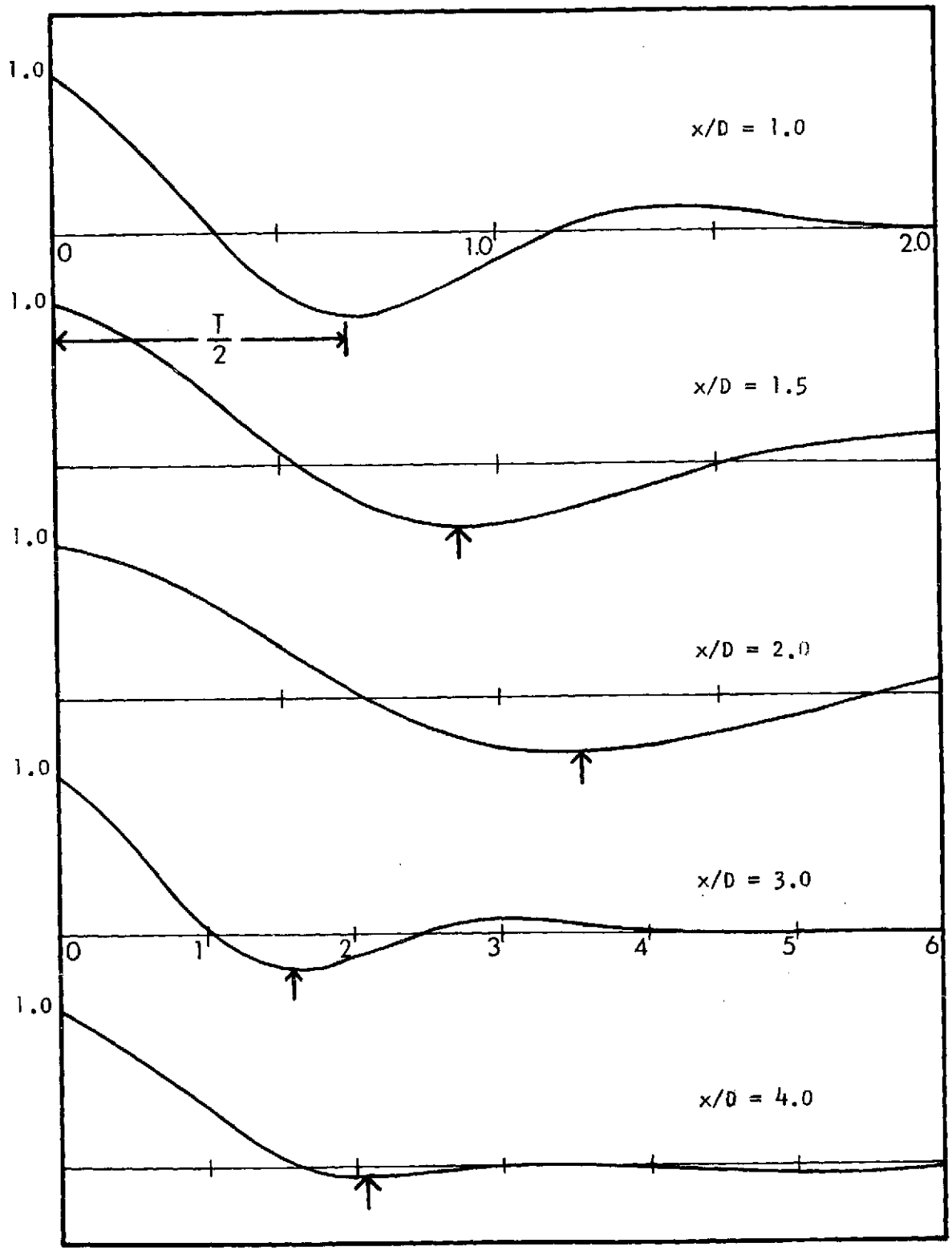

Auto-correlation, $\frac{\overline{p_A p_A(\tau)}}{p_A'^2}$, (dimensionless)

Time delay, τ, msec

(a) Axial stations, x/D, 1.0 to 4.0.

Figure 2. -Auto-correlation of pressure signals measured at various stations along edge of jet. The arrows (↑) denote the time of the first minimum. Radial positions lie along 10° cone.

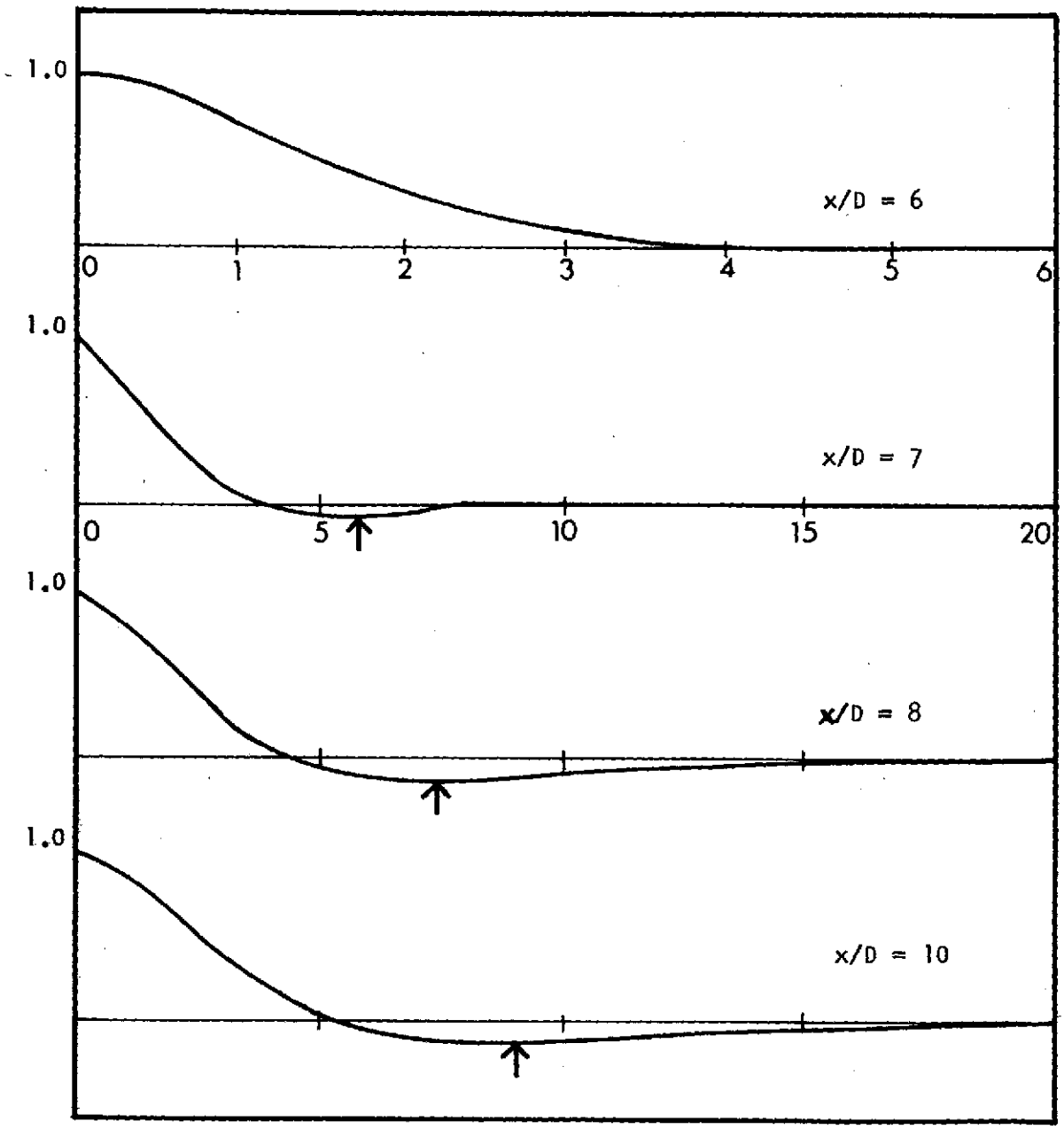

Auto-correlation, $\frac{\overline{P_A P_A(\tau)}}{P_A'^2}$, (dimensionless)

Time delay, τ, msec.

(b) Axial stations, x/D, 6 to 10

Figure 2. -Concluded.

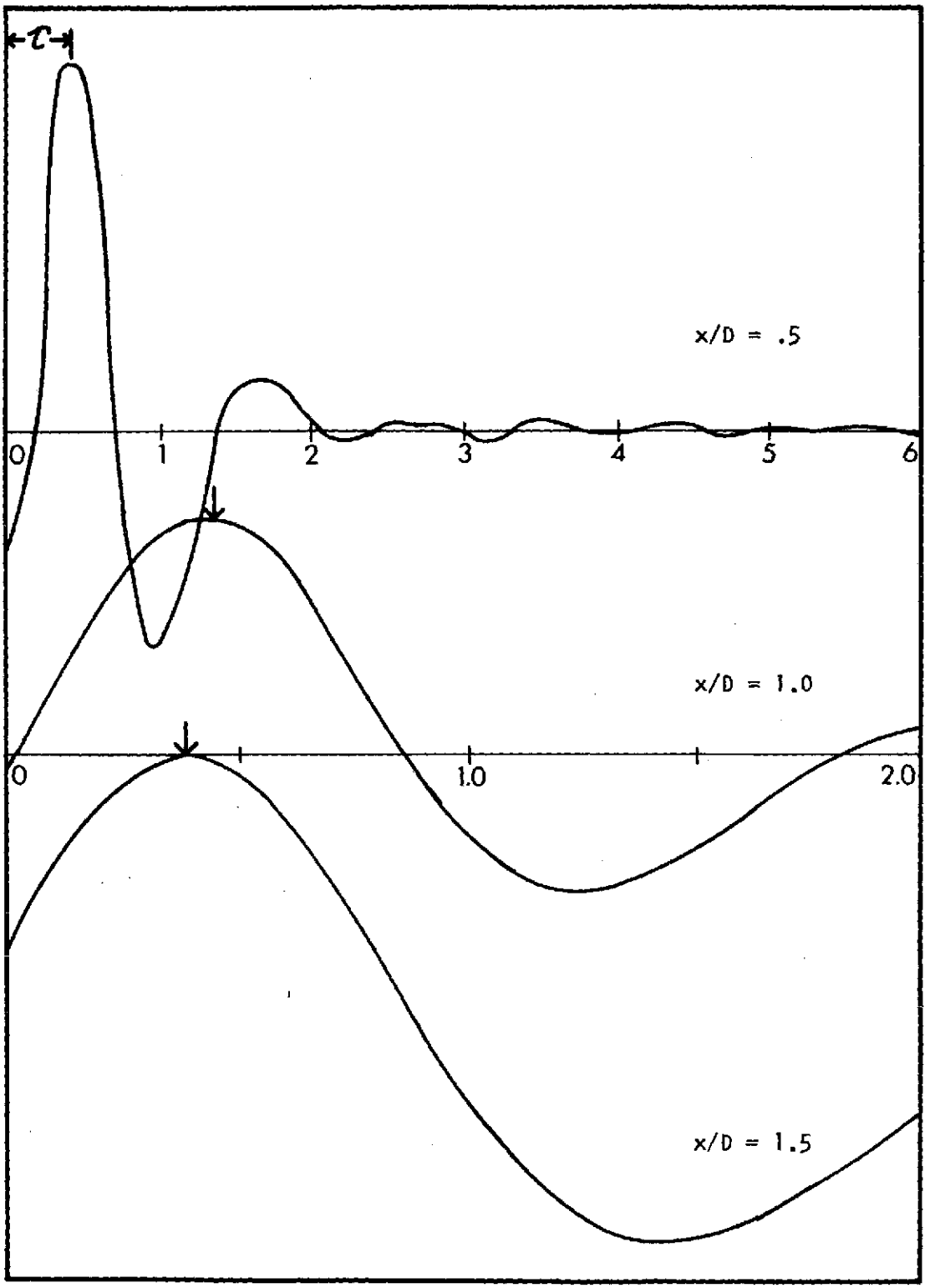

(a) Axial stations, x/D , .5 to 1.5.

Figure 3. -Axial cross-correlations of pressure signals at various stations along edge of jet. Arrows (↑) denote time of maximum cross correlation. Radial positions lie along 10° cone.

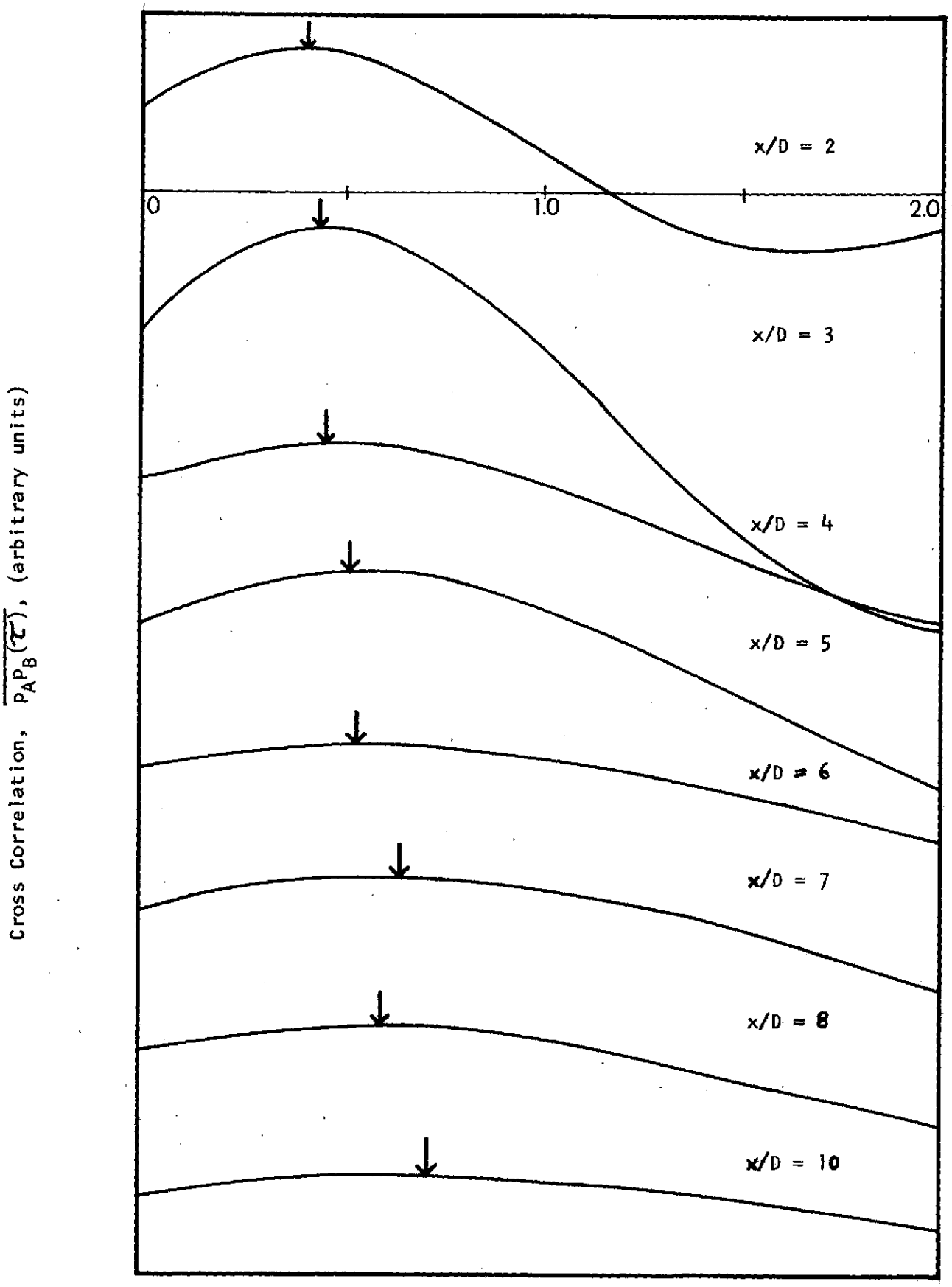

-29-

(b) Axial stations, x/D , 2 to 10.

Figure 3. - Concluded.

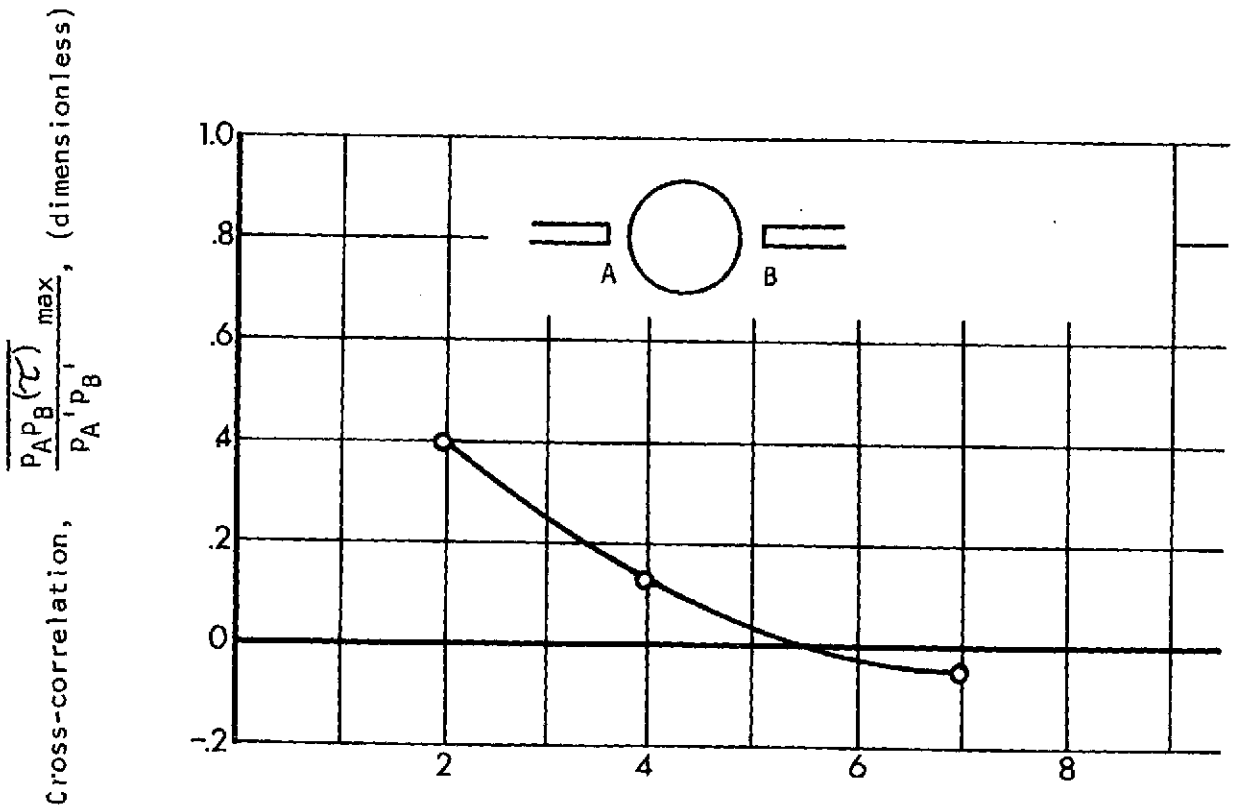

Figure 4. - Maximum of azimuthal cross-correlations of pressure signal measured across the jet along a cone angle of 10^{o}.

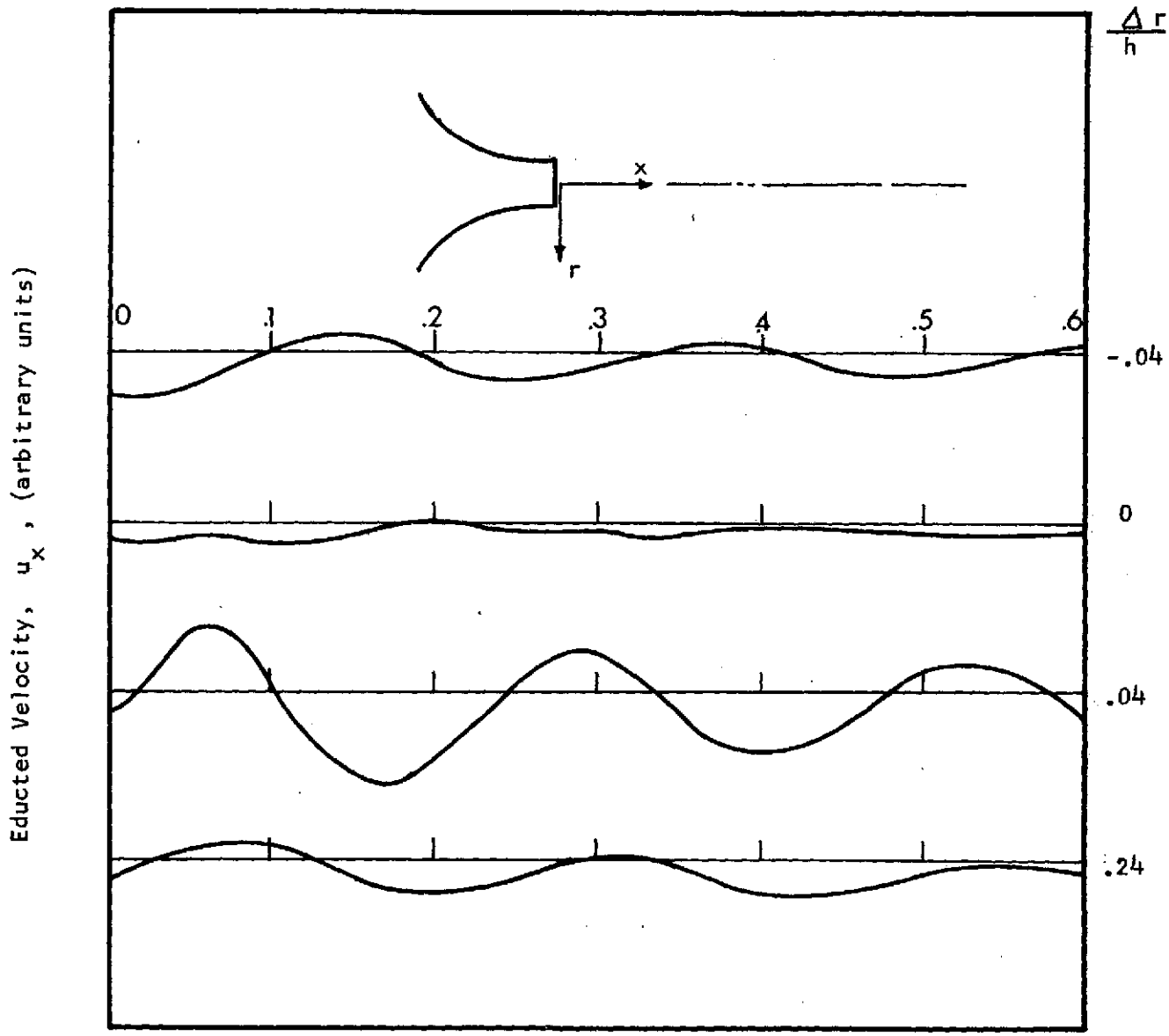

(a) x/D = .20; $\Delta r/h$, -0.04 to 0.24

Figure 5. - Educted Axial Velocity Signatures across the Shear Layer.

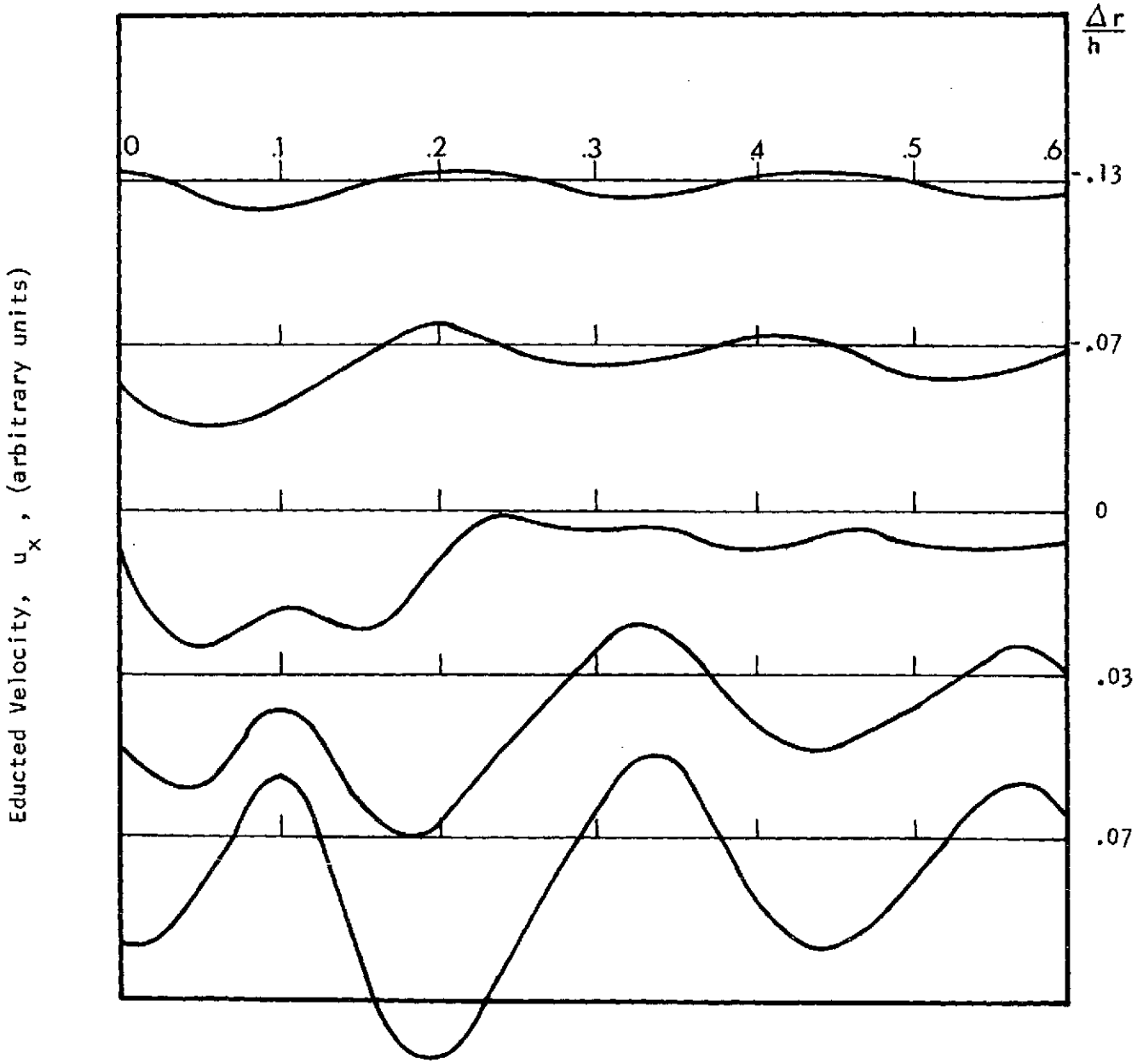

(b) x/D = .28 ; Δ r/h , -0.13 to 0.07

Figure 5. - Continued.

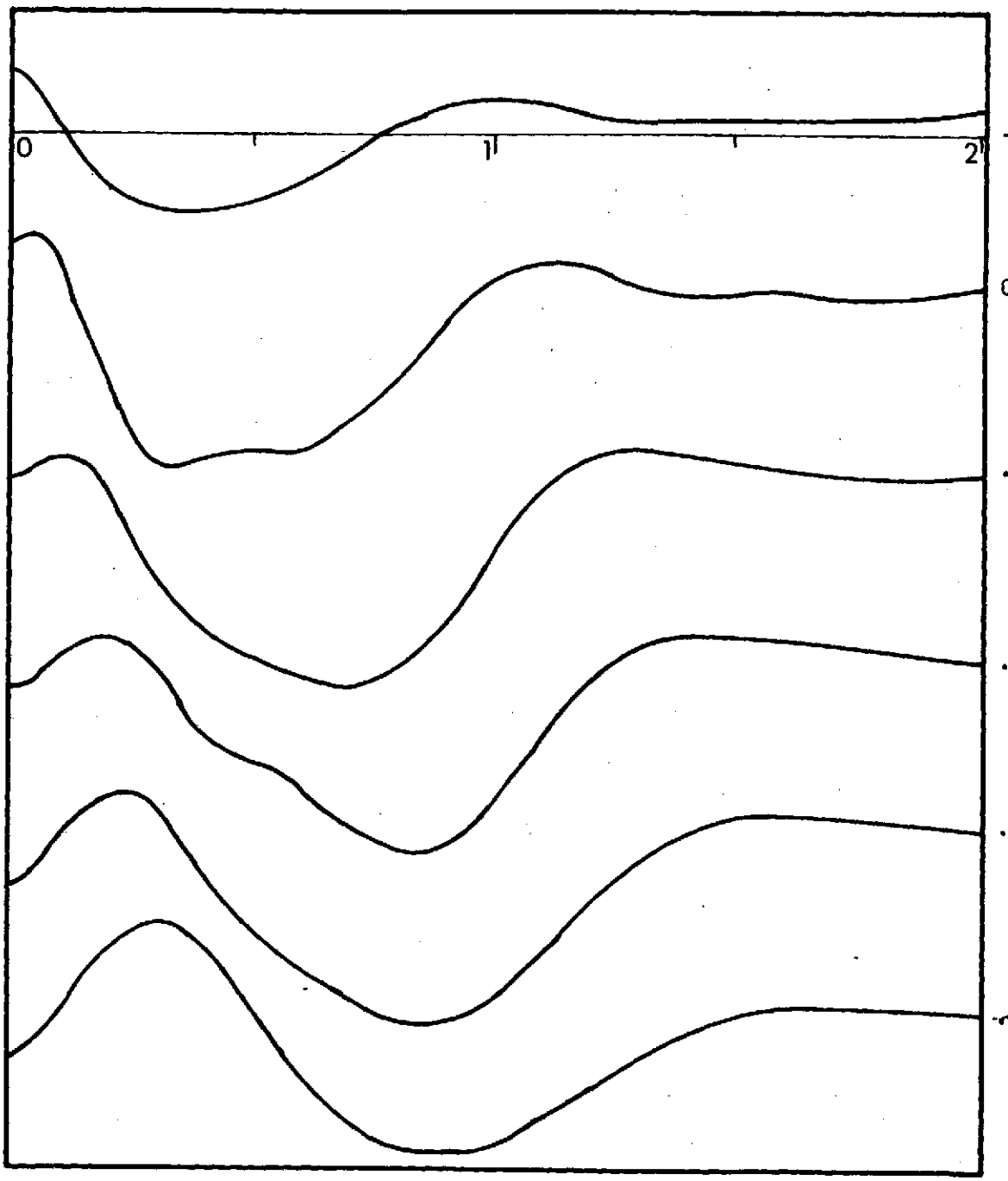

(c) x/D = 0.9 ; Δ r/h, -0.16 to 0.63

Figure 5. - Continued.

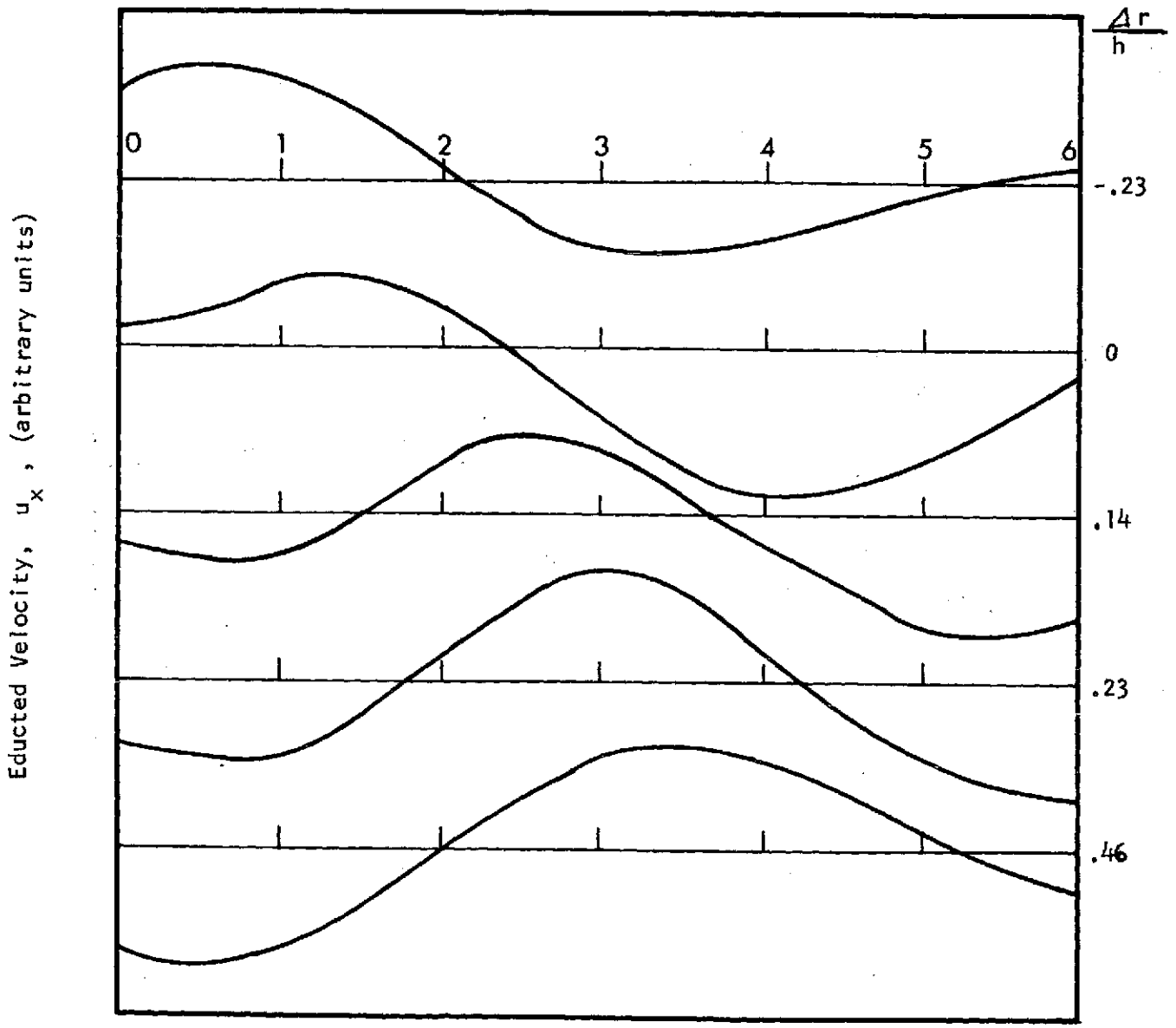

(d) x/D = 4 ; Δ r/h, -0.23 to 0.46

Figure 5. - Continued.

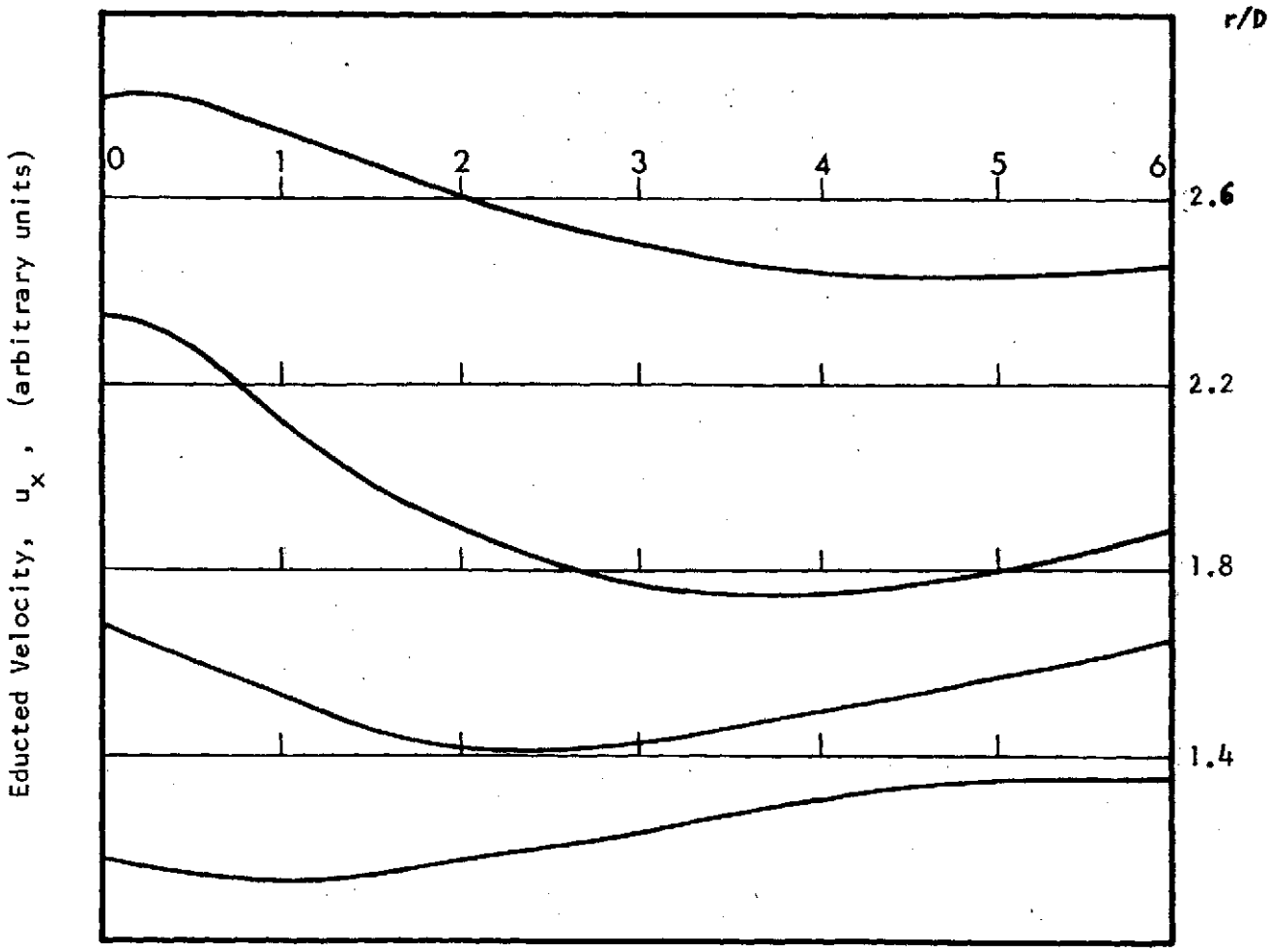

(e) x/D = 9 ; r/D, 1.4 to 2.6

Figure 5. - Concluded.

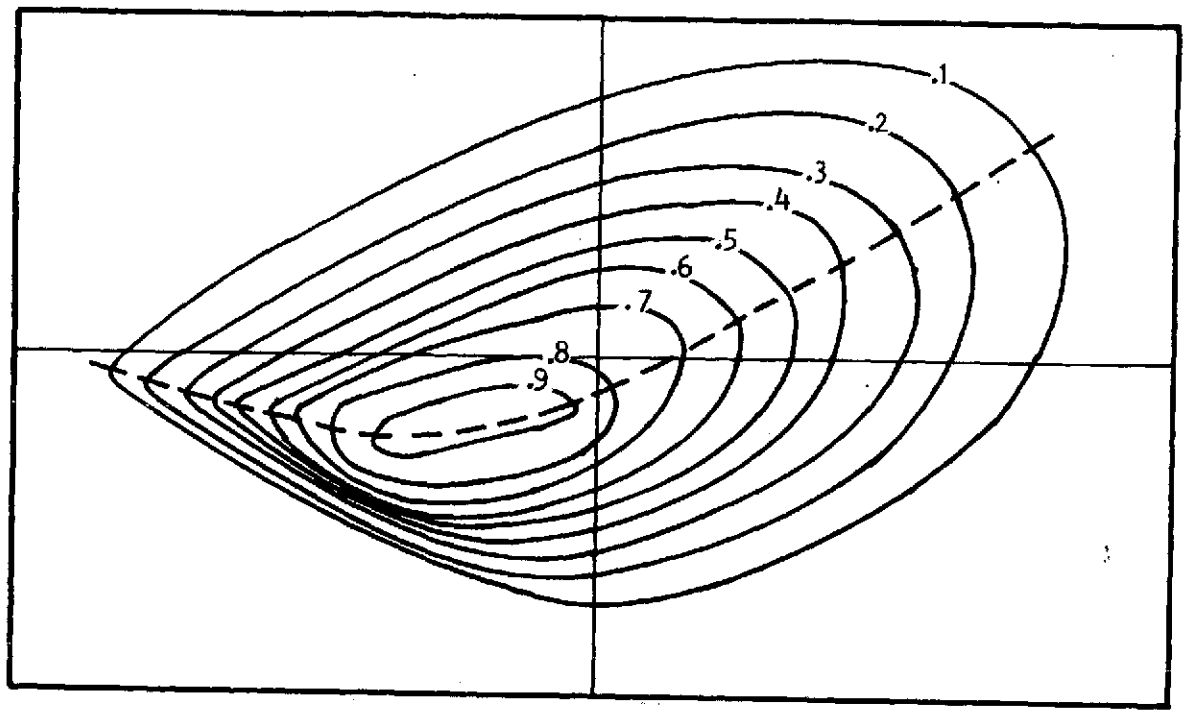

Radial velocity fluctuation, $u_r - \bar{u}_r$, (relative units)

Axial velocity fluctuation, $u_x - \bar{u}_x$, (relative units)

(a) $r/D = 0.56$; $\bar{u}/U_e = 0.60$

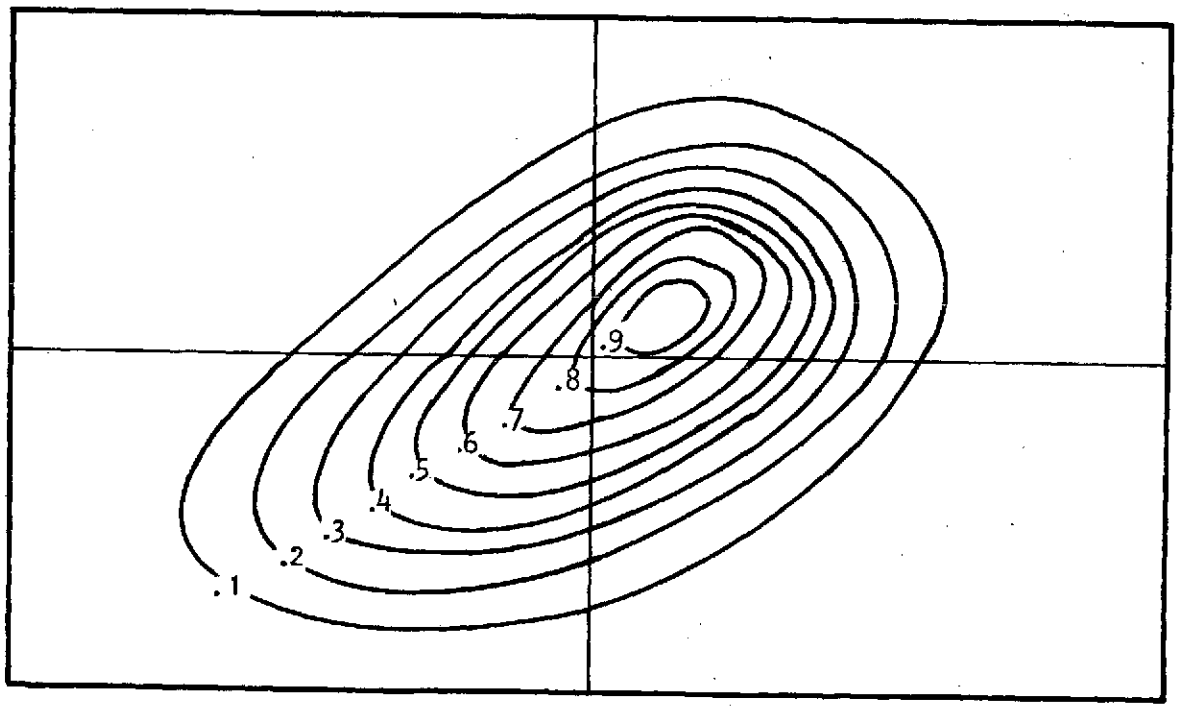

Radial velocity fluctuation, $u_r - \bar{u}_r$, (relative units)

Axial velocity fluctuation, $u_x - \bar{u}_x$, (relative units)

(b) $r/D = 0.49$; $\bar{u}/U_e = 0.79$

Figure 6. - Joint Probability Distributions $P(u_x, u_r)$. Isoprobability Contours shown for $x/D = 2$. Contour level shown as fraction of the distribution peak.

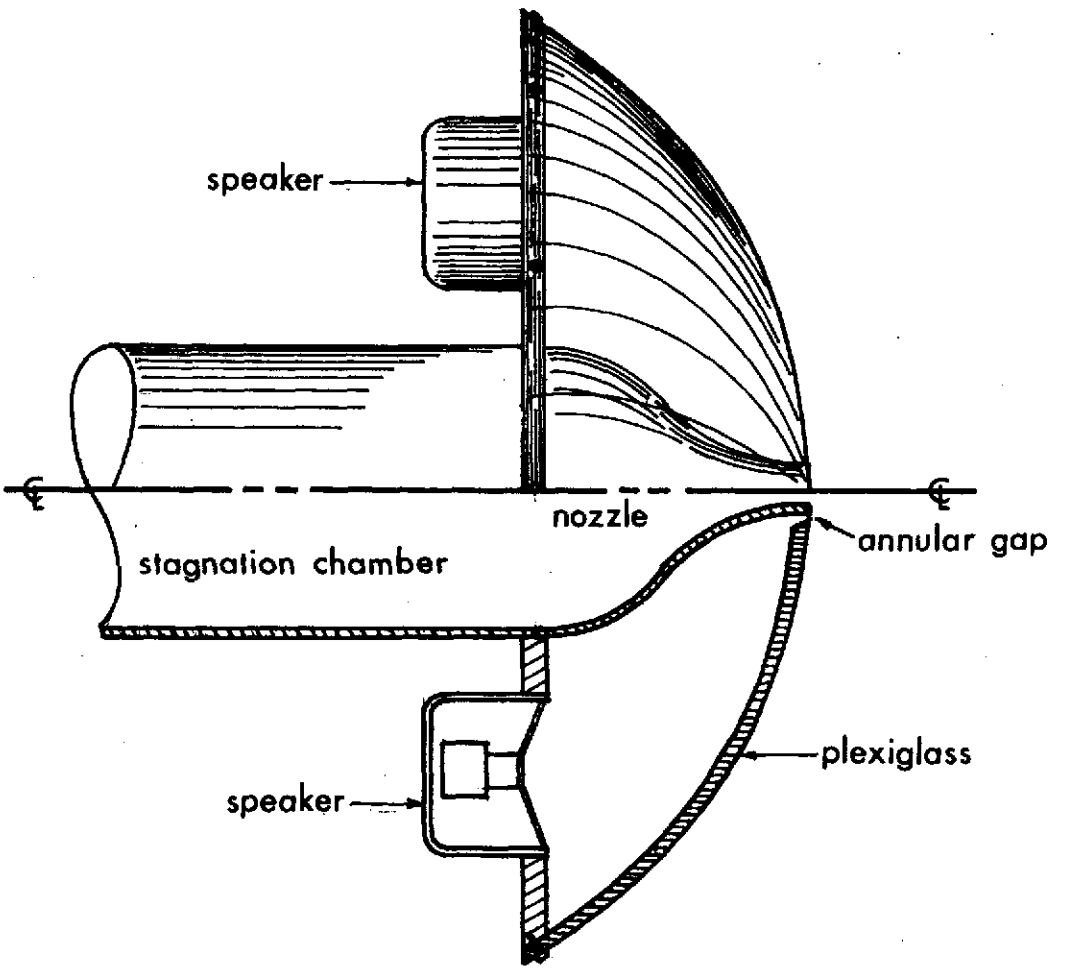

Figure 7. - Acoustic Driver Assembly.

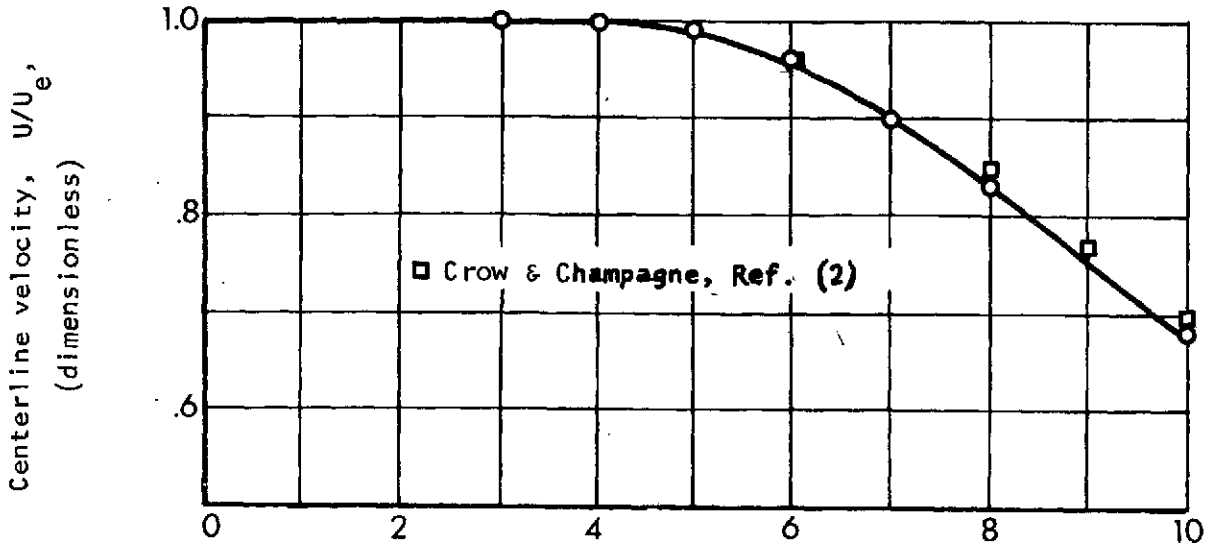

Figure 8. - Centerline Velocity Decay.

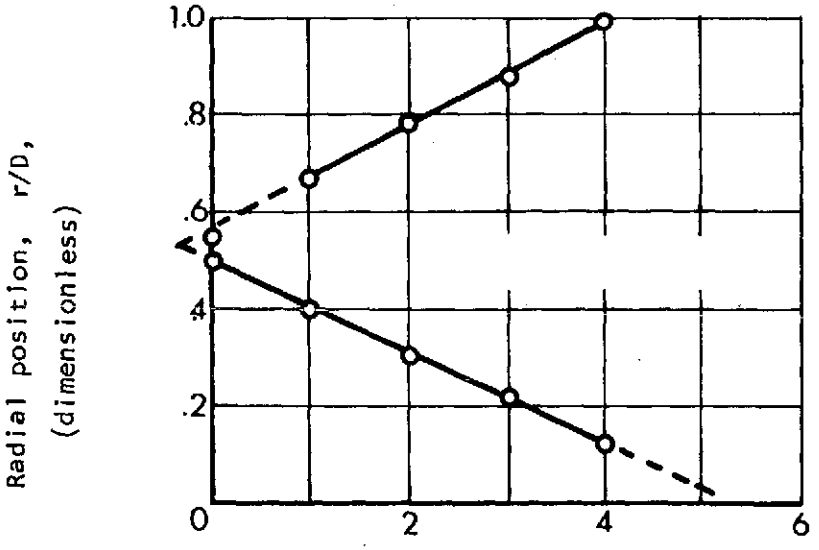

Upper trace is $\bar{u}/U_e = .10$

Lower trace is $\bar{u}/U_e = .99$

Shear layer thickness h is distance between lines.

Figure 9. - Shear Layer Growth.

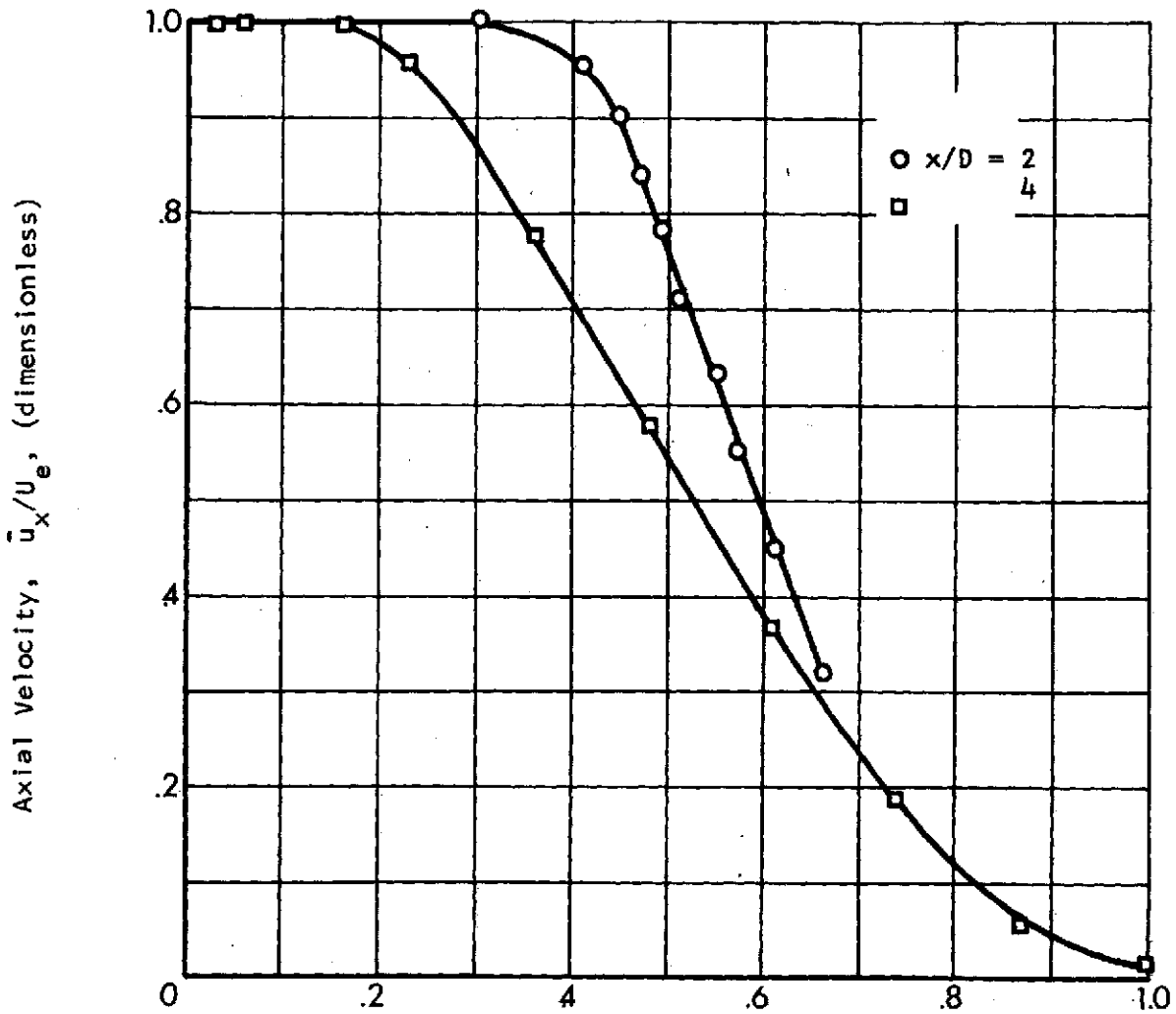

Figure 10. - Radial Velocity Profiles.

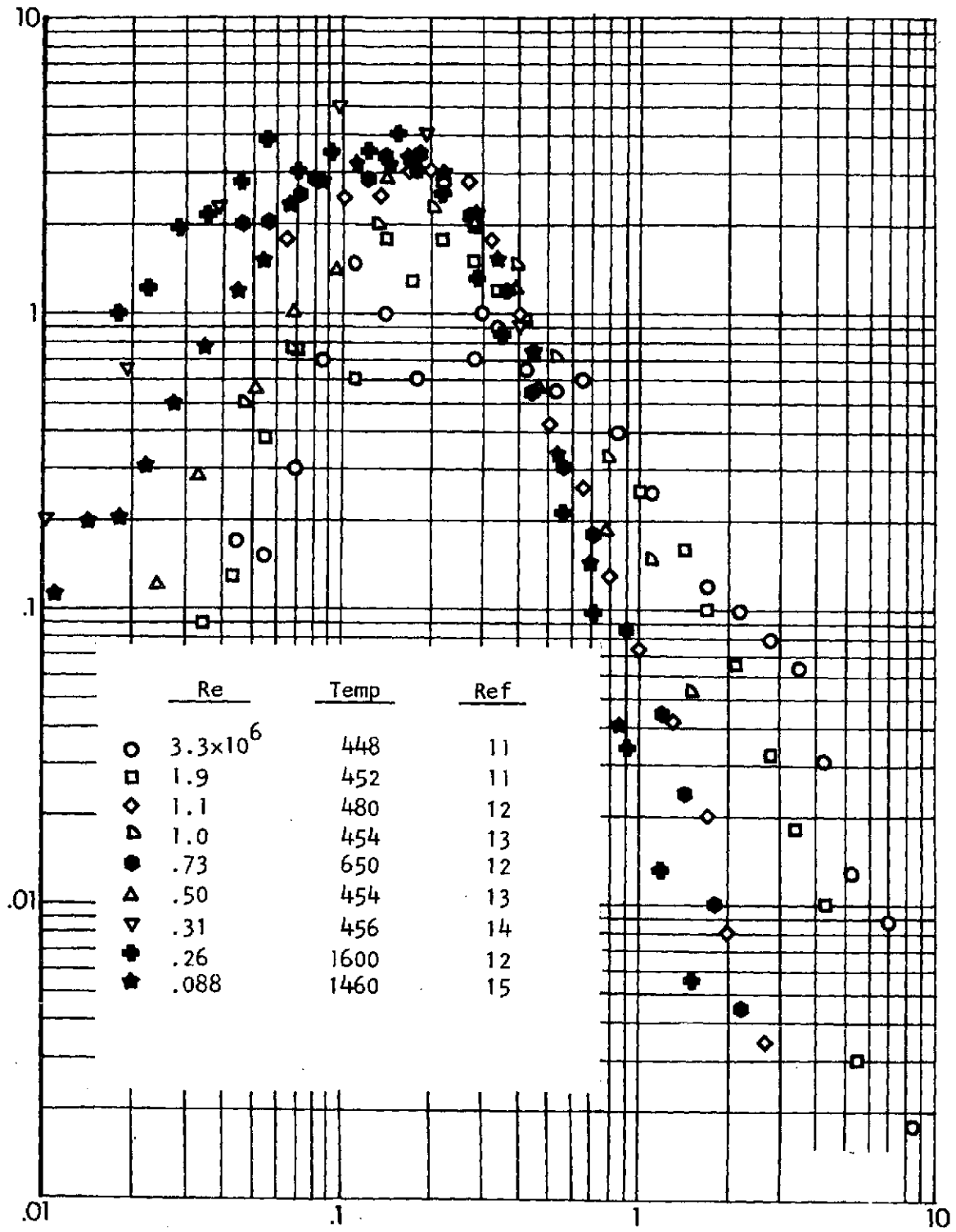

40

Figure 11. - Dimensionless overall power spectral density of jet noise. $M_e = 0.90 \pm 0.02$, Reynolds numbers 0.88 to 3.3×10^6.

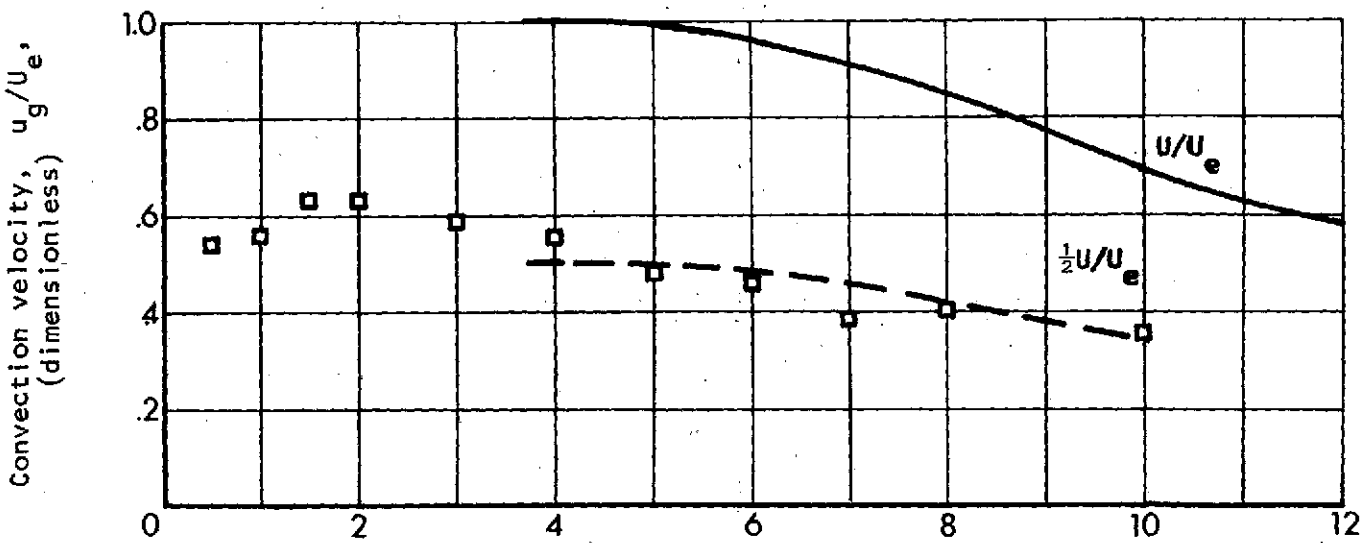

Axial position, x/D , (dimensionless)

Figure 12. - Turbulence Convection Velocity Decay.

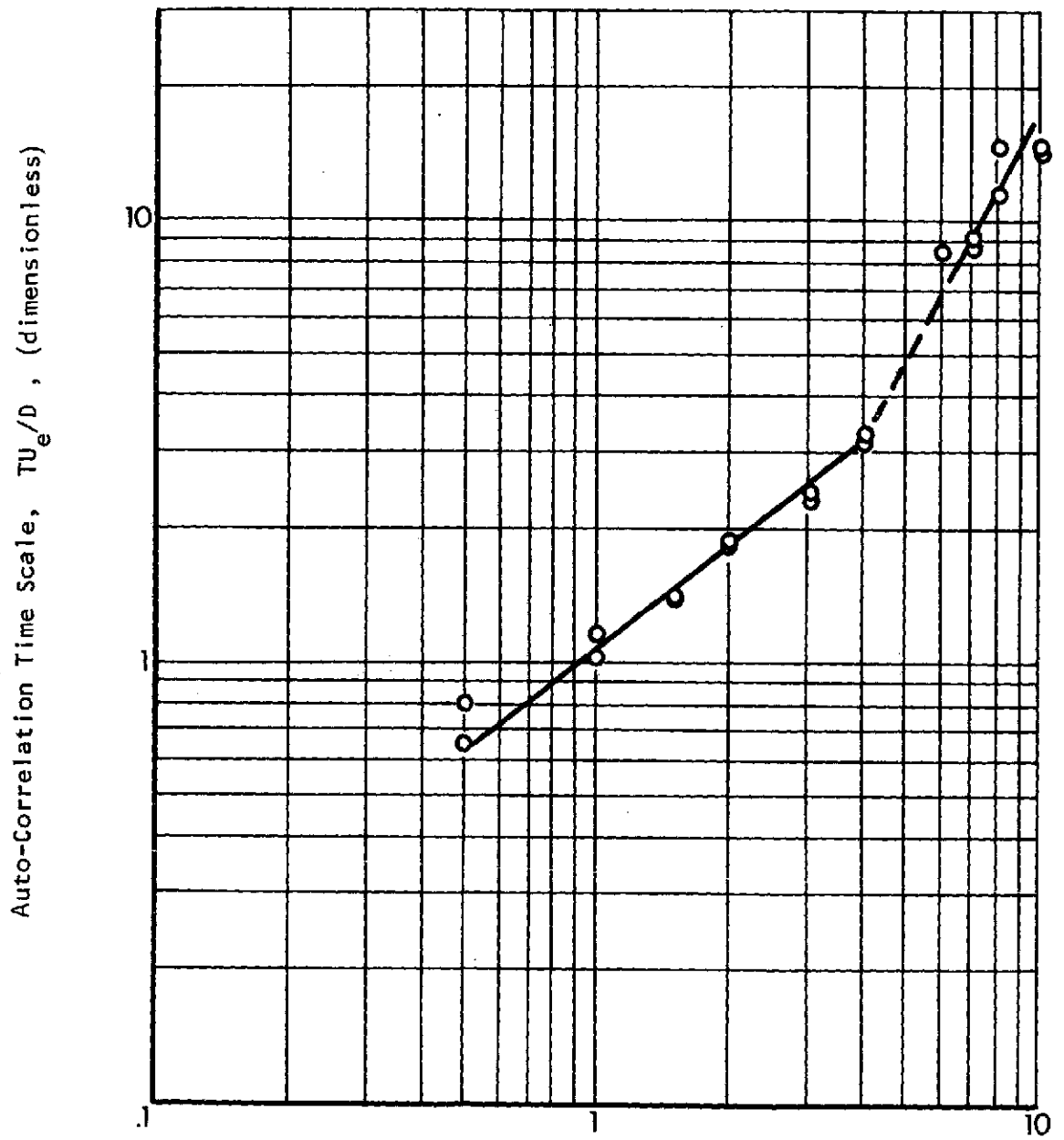

Figure 13. - Auto-Correlation Time Scale (T) vs. Downstream Station.

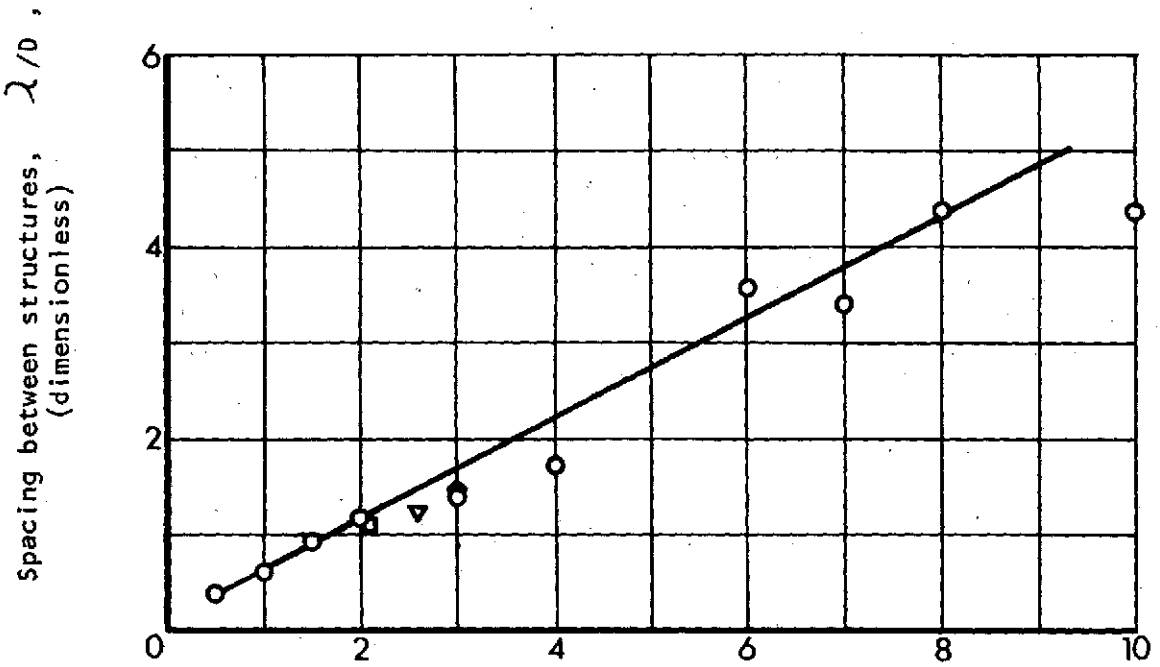

Figure 14. - Spacing Between Coherent Structures.

- ☐ Ko & Davis (Ref. 16)
- ◇ Fuchs (Ref. 17)
- ▽ Lau, Fisher, & Fuchs (Ref. 3)

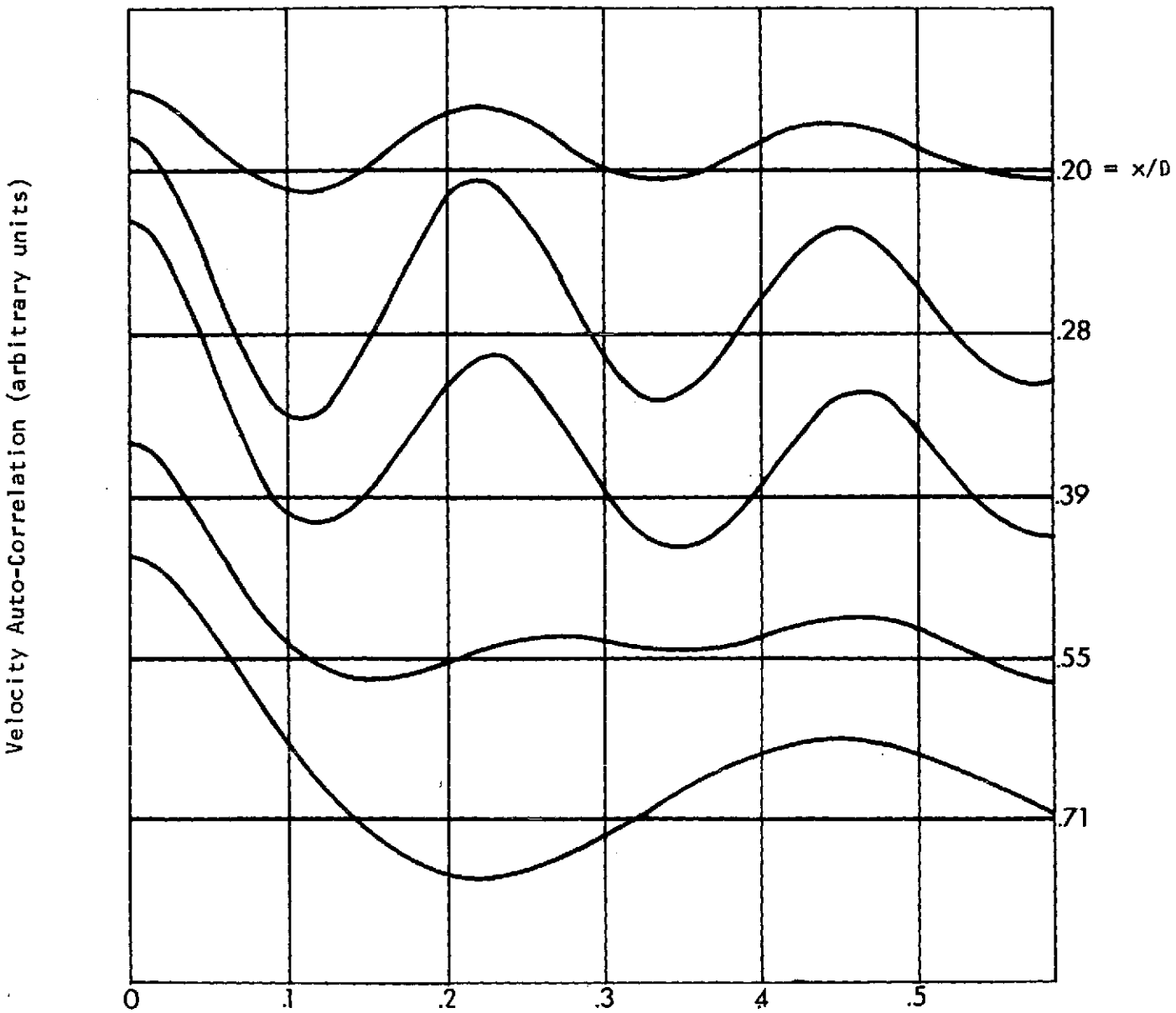

x/D, 0.20 to 0.70

Figure 15. - Auto-Correlations of Velocity Inside Shear Layer at Eigenmode Peak.

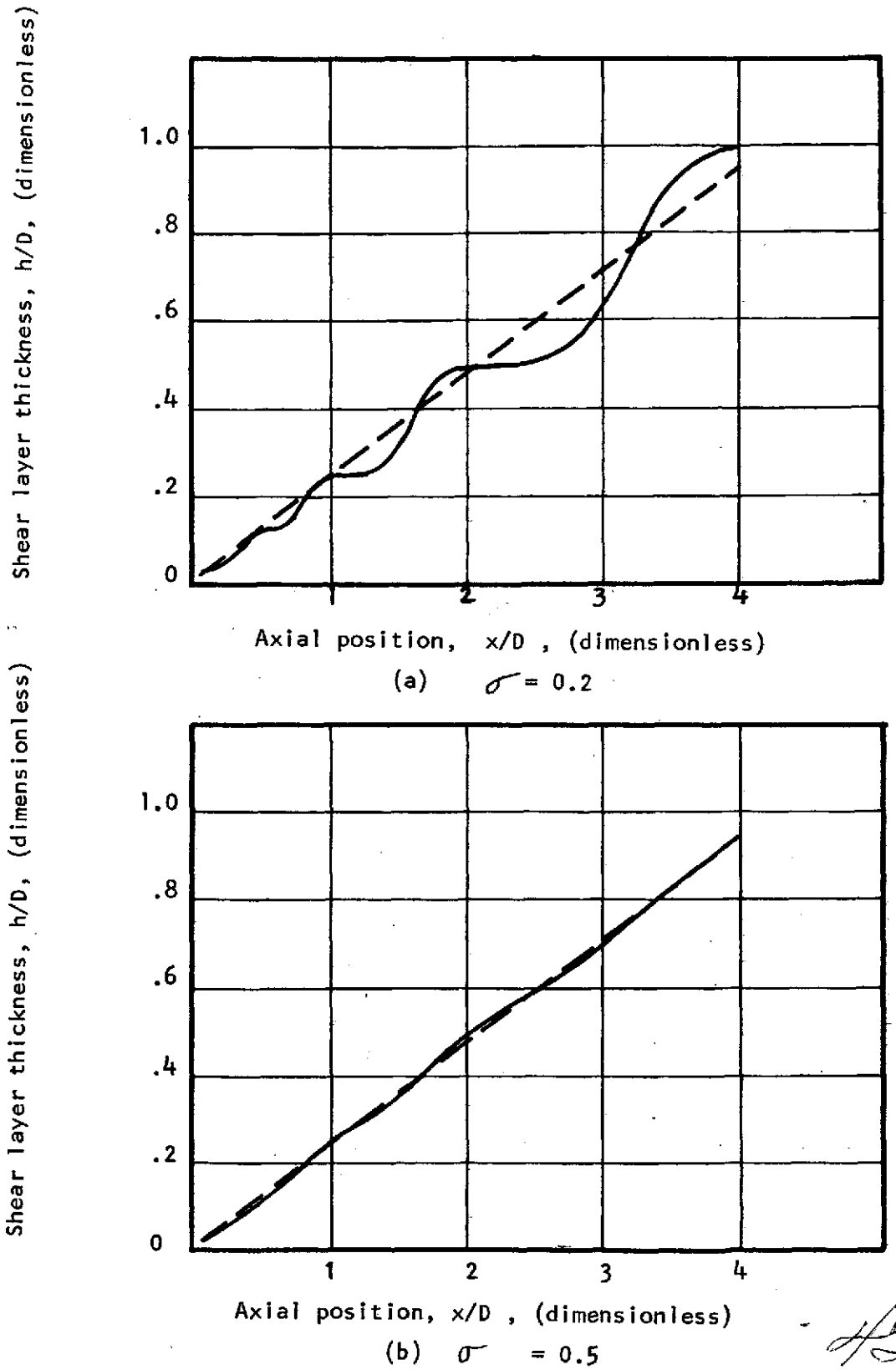

Figure 16. - Shear layer growth calculated according to Eq. (11): Effect of uncertainty in pairing location, σ .

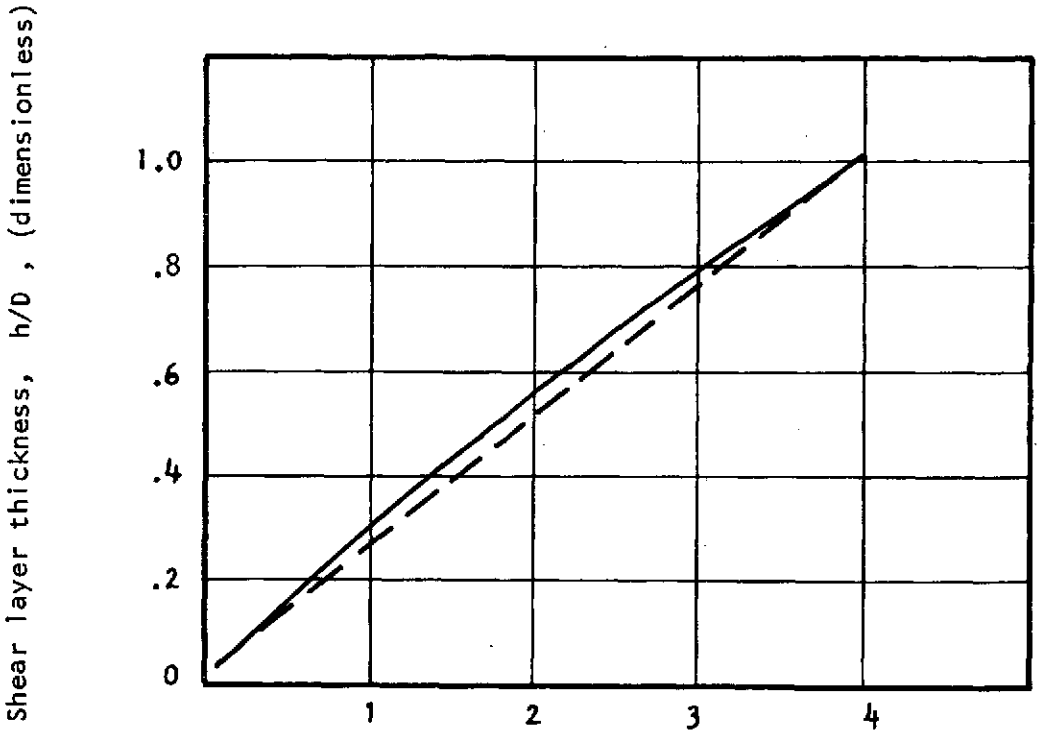

(c) σ = 1.0

Figure 16. - Concluded.

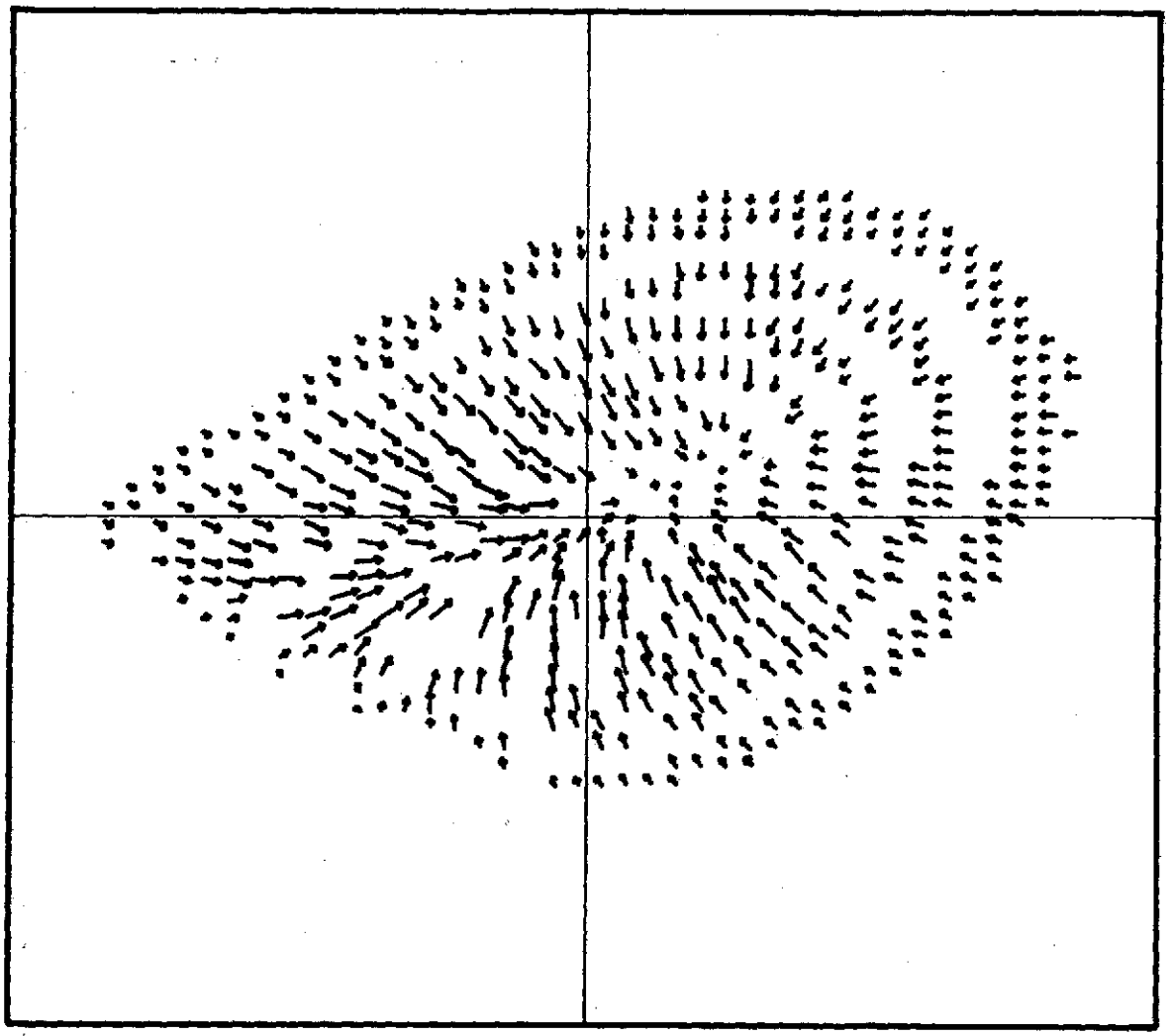

(a) r/D = 0.56; x/D = 2.0

Figure 17. - Experimentally measured expectation of velocity derivative $\underline{f}$ (Eq. 13). The relative magnitude and direction of $\underline{f}$ are indicated by the arrows (↑), and the pattern is modulated by the isoprobability contours (fig. 6).

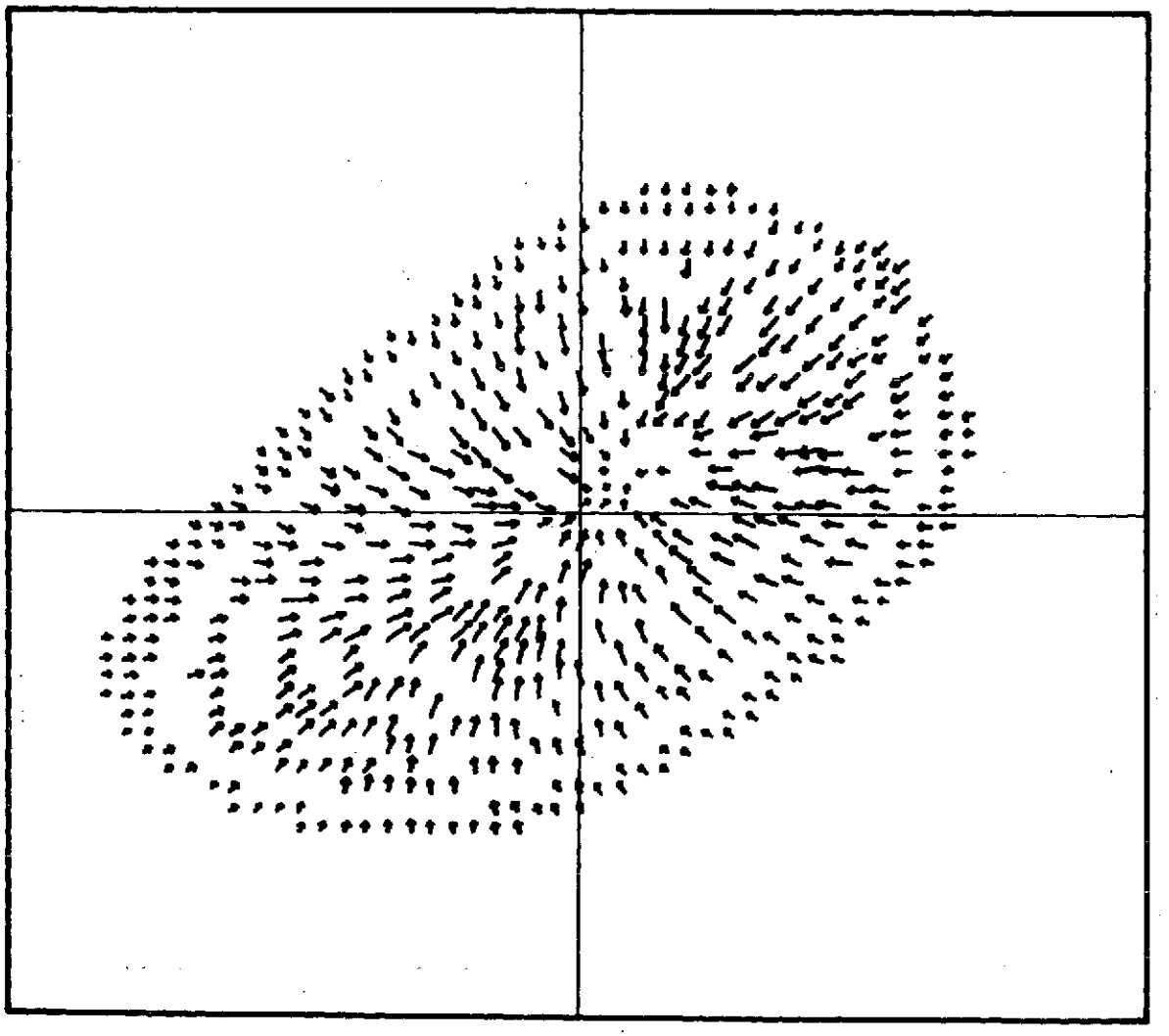

Axial velocity fluctuations, $u_x - \tilde{u}_x$, (relative units)

(b) r/D = 0.49; x/D = 2.0

Figure 17. - Concluded.

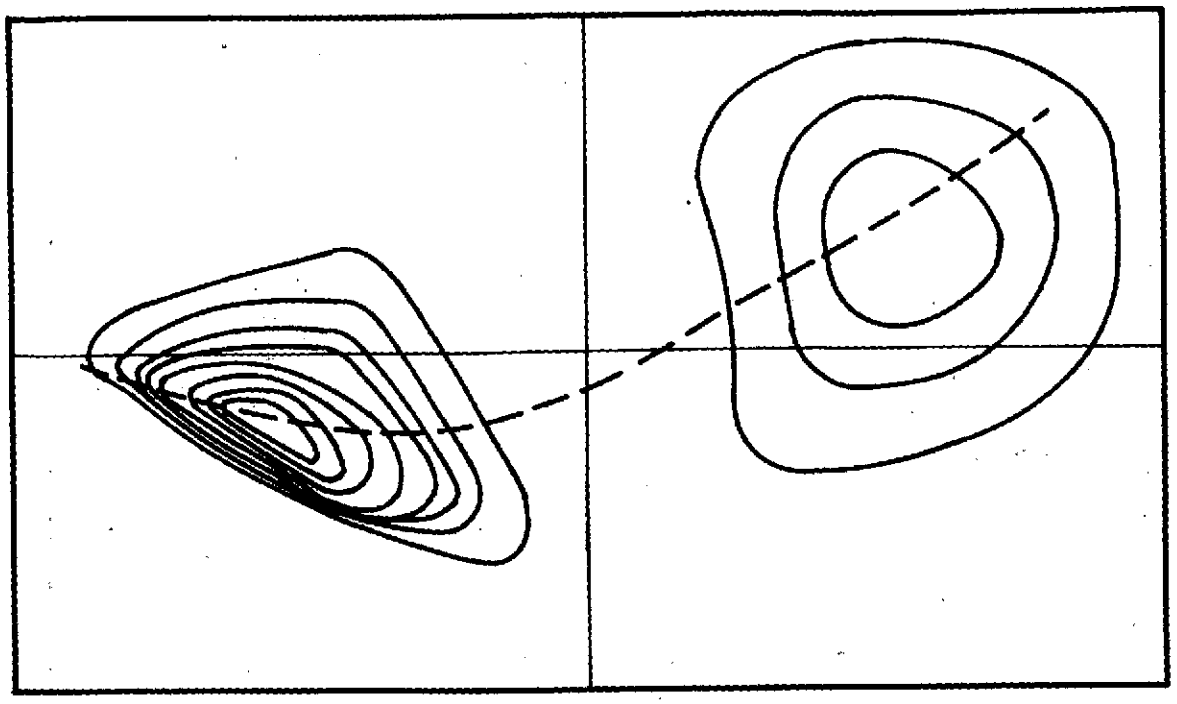

Axial velocity fluctuations, $u_x - \bar{u}_x$, (relative units)

r/D = .56; x/D = 2.0

Figure 18. - Turbulent Energy Isoprobability Density Contours.

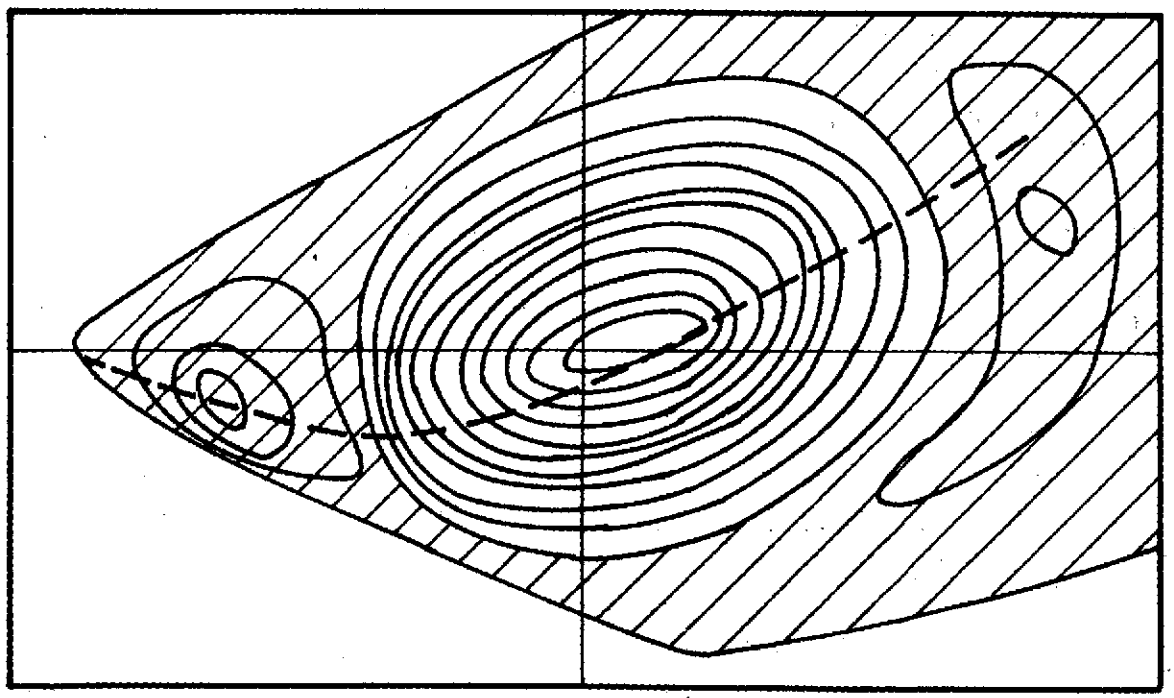

Axial velocity fluctuations, $u_x - \bar{u}_x$, (relative units)

-19-

Figure 19. - Turbulent Energy Transition Levels. Cross-Hatched Region Indicates Negative Transition Levels. Note: Contours at Equal Intervals.

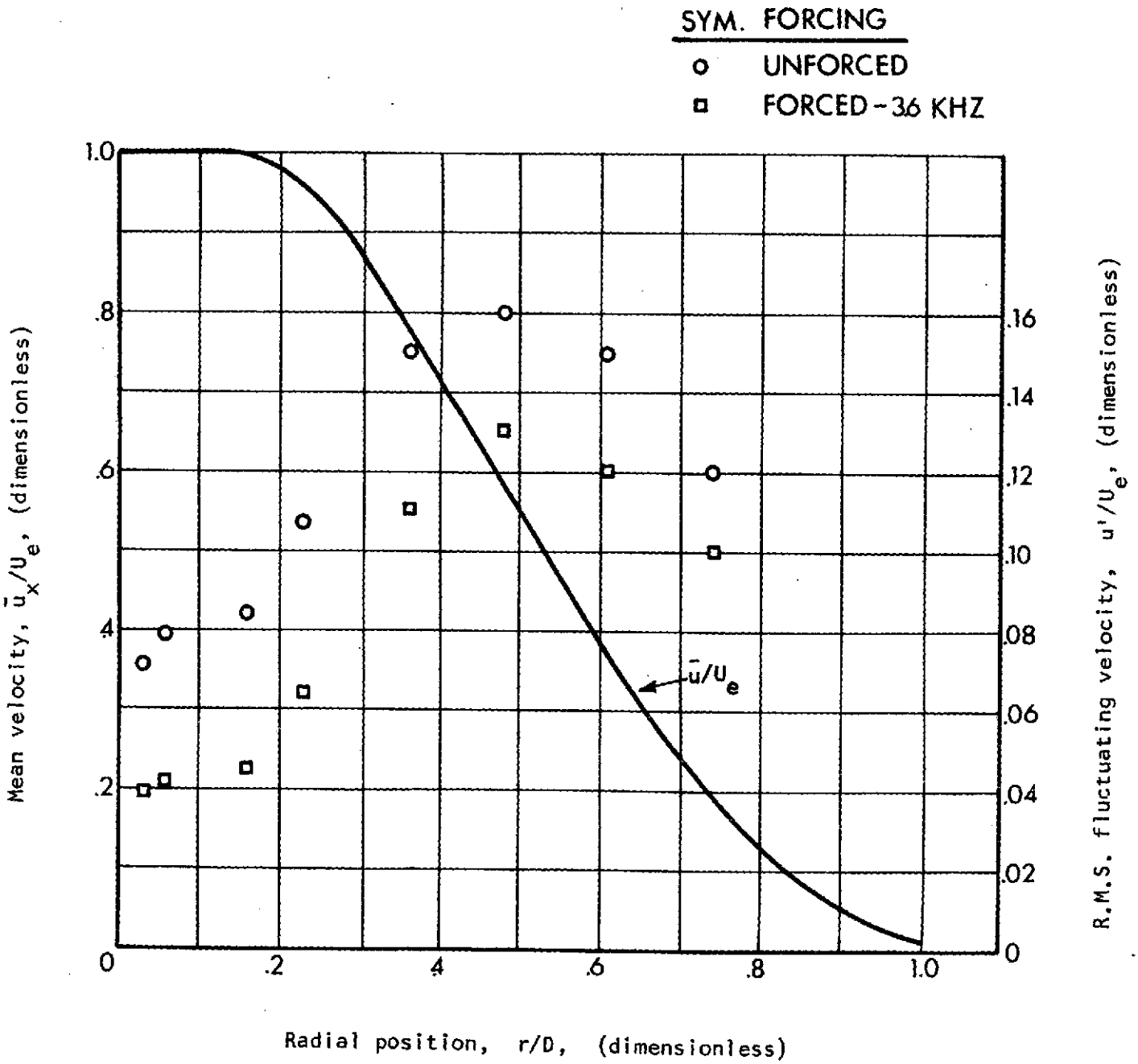

Figure 20. - Effect of Forcing on Shear Layer Turbulent Profiles. x/D = 4. Mean Profile Included for Reference.

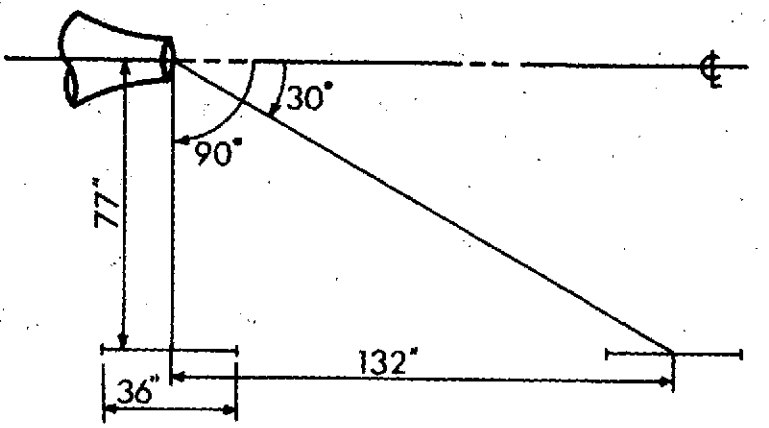

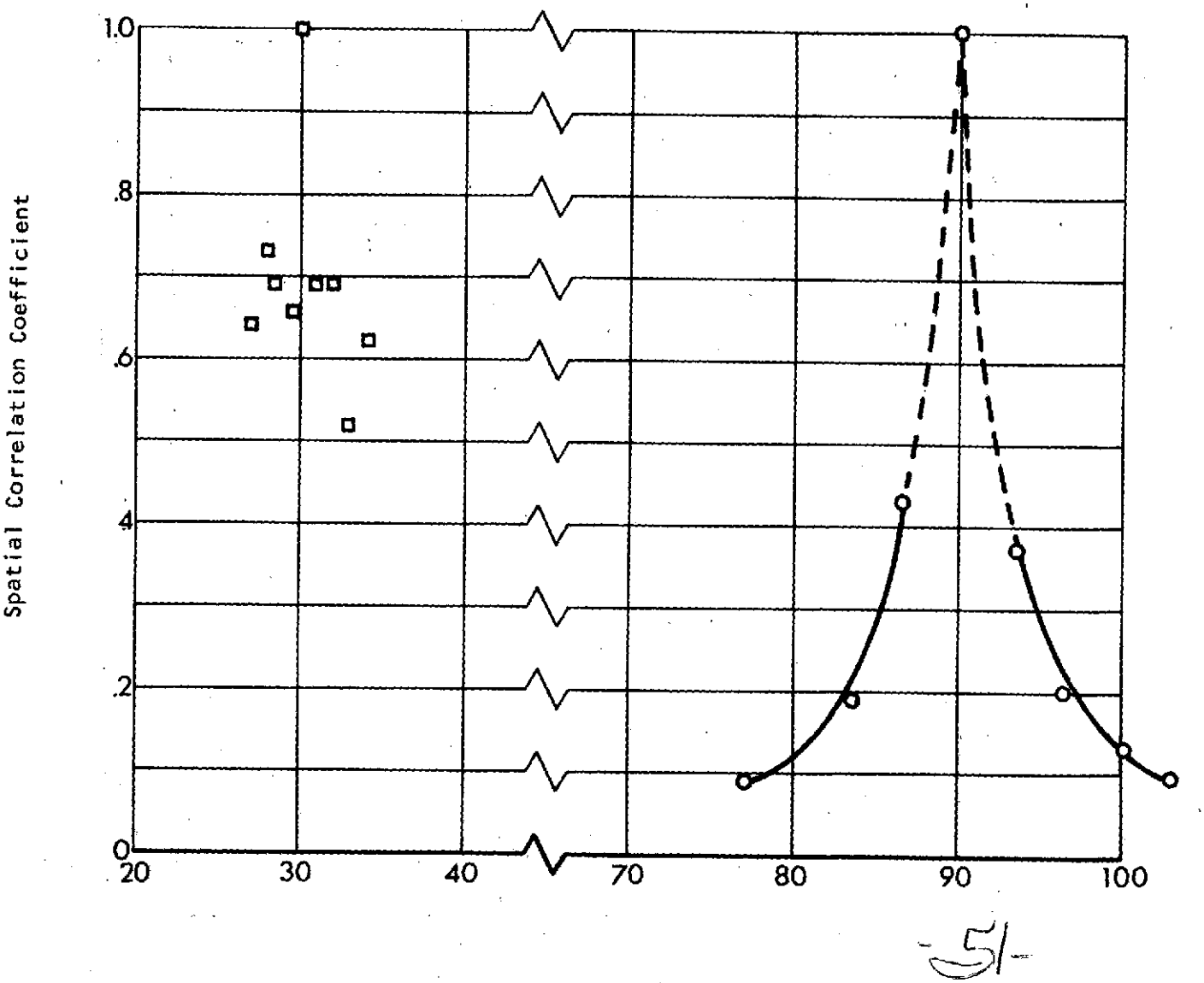

-51-

Polar Angle, degrees

Figure 21. - Far Field Acoustic Spatial Coherence.

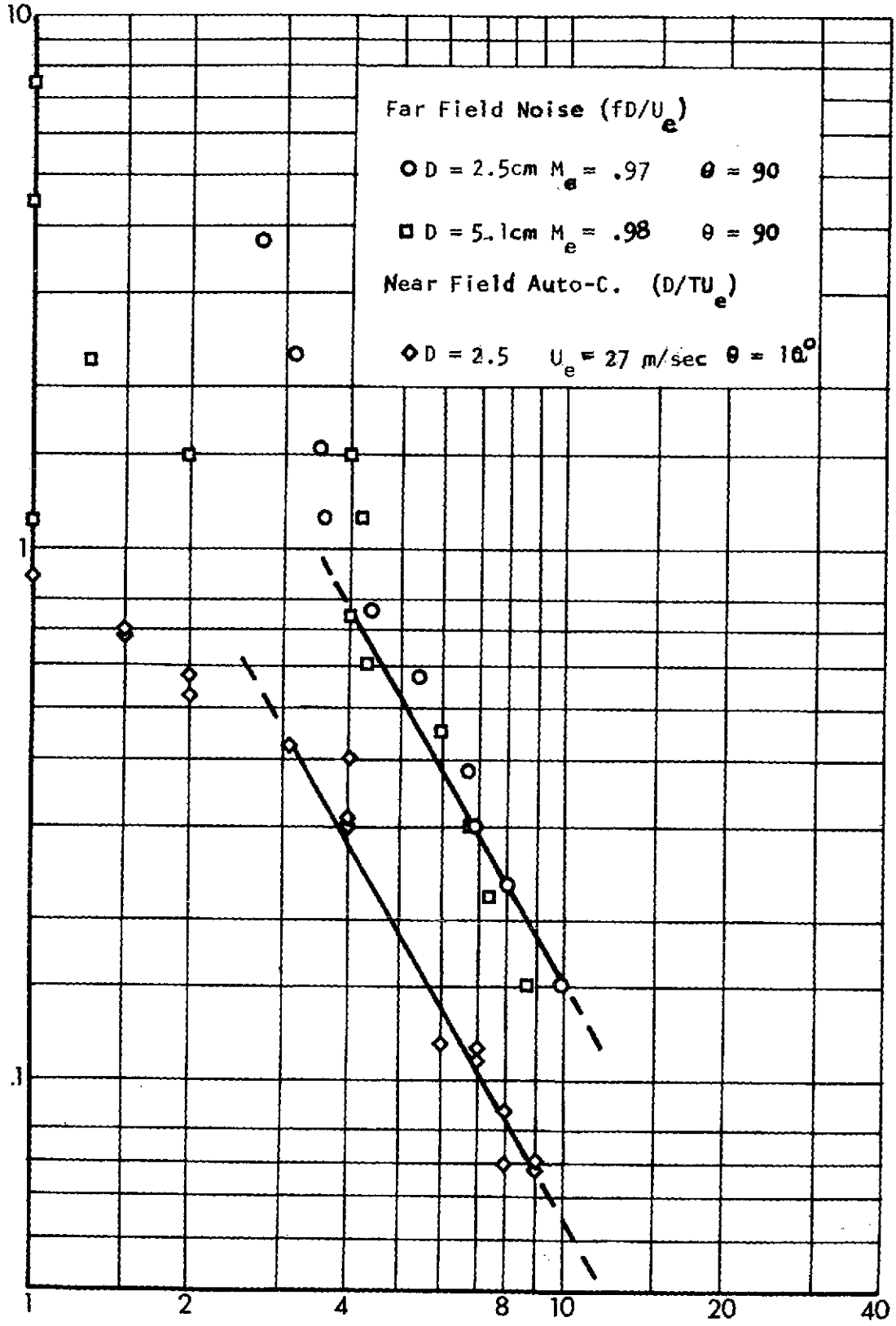

Figure 22. - Comparison of Near Field Time Scale (T) with characteristic far field acoustic frequency (f).

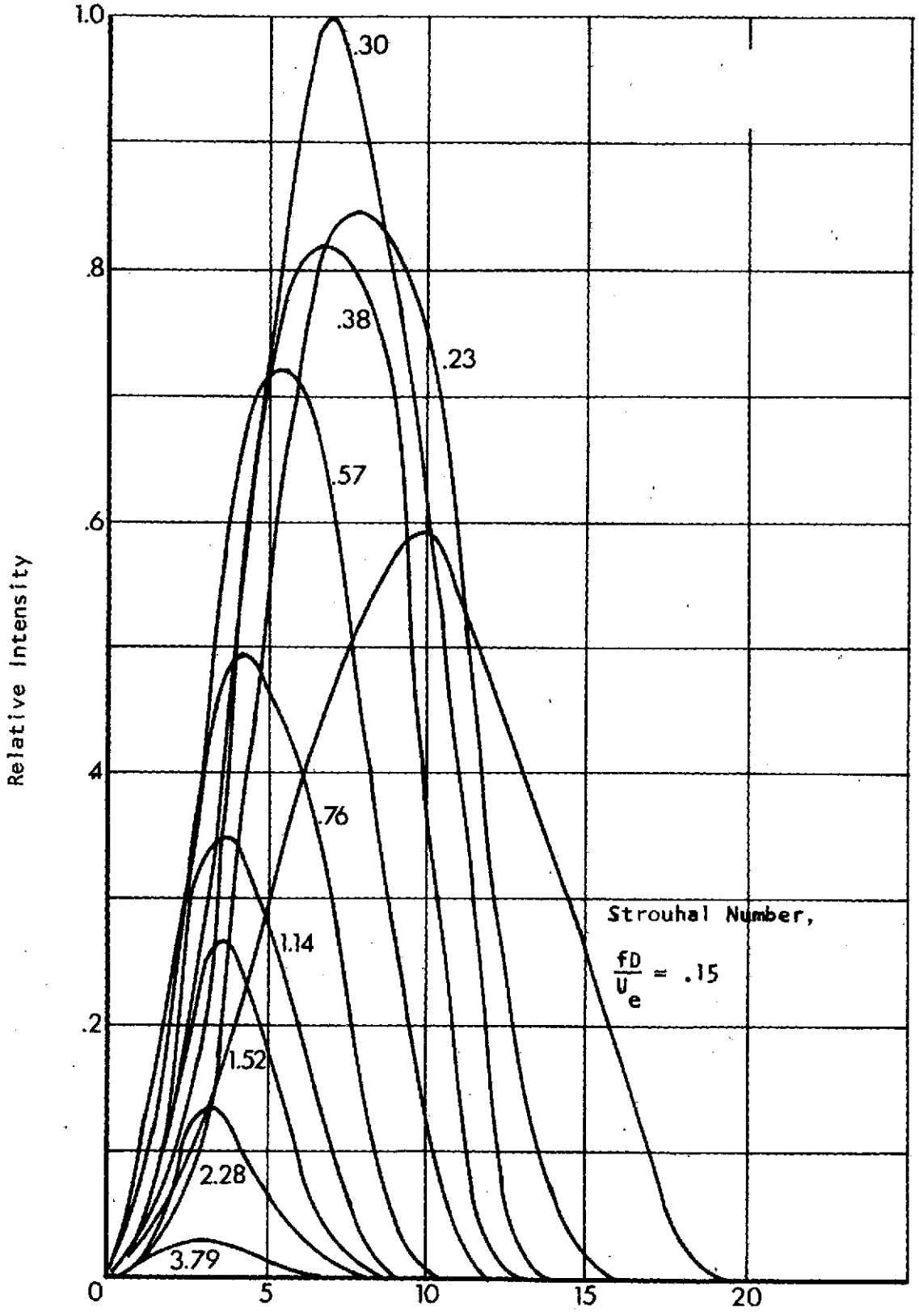

Axial location, x/D , (dimensionless)

Figure 23. - Processed, narrow band acoustic source intensity distributions along a 1", M_e = .97 jet, as seen by a reflector microphone in the far field normal to the jet axis.